© 2013. Published by The Company of Biologists Ltd | Development (2013) 140, 4624-4632 doi:10.1242/dev.099226

RESEARCH ARTICLE

TECHNIQUES AND RESOURCES

Visualizing developmentally programmed endoreplication in mammals using ubiquitin oscillators

Asako Sakaue-Sawano[1,2], Tetsushi Hoshida[1,2], Masahiro Yo[3], Reiko Takahashi[1], Kenji Ohtawa[4], Takashi Arai[4], Eiki Takahashi[4], Shinichi Noda[3], Hiroyuki Miyoshi[3] and Atsushi Miyawaki[1,2,*]

ABSTRACT

The majority of mammalian somatic cells maintain a diploid genome. However, some mammalian cell types undergo multiple rounds of genome replication (endoreplication) as part of normal development and differentiation. For example, trophoblast giant cells (TGCs) in the placenta become polyploid through endoreduplication (bypassed mitosis), and megakaryocytes (MKCs) in the bone marrow become polyploid through endomitosis (abortive mitosis). During the normal mitotic cell cycle, geminin and Cdt1 are involved in 'licensing' of replication origins, which ensures that replication occurs only once in a cell cycle. Their protein accumulation is directly regulated by two E3 ubiquitin ligase activities, APC^{Cdh1} and SCF^{Skp2}, which oscillate reciprocally during the cell cycle. Although proteolysis-mediated, oscillatory accumulation of proteins has been documented in endoreplicating *Drosophila* cells, it is not known whether the ubiquitin oscillators that control normal cell cycle transitions also function during mammalian endoreplication. In this study, we used transgenic mice expressing Fucci fluorescent cell-cycle probes that report the activity of APC^{Cdh1} and SCF^{Skp2}. By performing long-term, high temporal-resolution Fucci imaging, we were able to visualize reciprocal activation of APC^{Cdh1} and SCF^{Skp2} in differentiating TGCs and MKCs grown in our custom-designed culture wells. We found that TGCs and MKCs both skip cytokinesis, but in different ways, and that the reciprocal activation of the ubiquitin oscillators in MKCs varies with the polyploidy level. We also obtained three-dimensional reconstructions of highly polyploid TGCs in whole, fixed mouse placentas. Thus, the Fucci technique is able to reveal the spatiotemporal regulation of the endoreplicative cell cycle during differentiation.

KEY WORDS: Fucci imaging, Endomitosis, Endoreduplication

INTRODUCTION

Endoreplication is the process by which a cell undergoes successive rounds of DNA replication without intervening mitosis or cytokinesis, resulting in polyploidy (Zybina and Zybina, 1996; Edgar and Orr-Weaver, 2001; Lee et al., 2009; Ullah et al., 2009; Hu and Cross, 2010; Davoli and de Lange, 2011). In lower eukaryotes, endoreplication is developmentally programmed and is a major phenomenon during embryogenesis and differentiation. For example, salivary gland and follicle cells in *Drosophila* and leaf epidermal cells in plants have polyploid nuclei (Schaeffer et al., 2004; Lammens et al., 2008; Narbonne-Reveau et al., 2008). In these cell types, anaphase-promoting complex/cyclosome (APC/C) and an activator (Cdh1, Fzr or ccs52a) are required to switch from the mitotic to the endoreplicative state. The cyclic activity of $APC/C^{Cdh1/Fzr/ccs52a}$ is also essential to sustain endoreplication.

Endoreplication is a relatively minor event in mammals and has been intensively studied in two cell types. Trophoblast giant cells (TGCs) and megakaryocytes (MKCs) undergo endoreduplication (bypassed mitosis) and endomitosis (abortive mitosis), respectively. TGCs are polyploid cells in the placenta that are essential for embryonic implantation in the uterus and for post-implantation placental development. TGCs avoid mitosis entirely, and this form of endoreplication is called endoreduplication. TGCs endoreduplicate as they differentiate from trophoblast stem cells (TSCs) in the trophectoderm layer of the blastocyst-stage embryo (Zybina and Zybina, 1996; Rossant and Cross, 2001; Martindill and Riley, 2008; Ullah et al., 2008; Ullah et al., 2009; Hu and Cross, 2010; Davoli and de Lange, 2011; Chen et al., 2012). Loss of fibroblast growth factor 4 (Fgf4) signaling or activation of the transcription factors Hand1 and Tead4 is necessary for TSCs to switch from the mitotic to the endoreduplicative cell cycle (Rossant and Cross, 2001; Martindill and Riley, 2008; Nishioka et al., 2008; Ullah et al., 2008; Chen et al., 2012). However, little is known about the molecular mechanisms responsible for progression of endoreduplication in TSCs.

MKCs in the bone marrow also show polyploidy. Hematopoietic stem cells (HSCs) differentiate first into megakaryoblasts (MKBs) and then into mature MKCs through endomitosis in the presence of the cytokine thrombopoietin (TPO; also known as THPO). Endomitosis is a form of endoreplication in which the cell undergoes early mitotic events such as chromosome condensation. Molecular candidates for the endomitotic switch include cyclin B1 and cyclin E (Carow et al., 2001; Bermejo et al., 2002; Eliades et al., 2010). In addition, live-imaging experiments were performed using the histone2B (H2B)-GFP or YFP-tubulin marker to monitor how mitosis aborted (Geddis et al., 2007; Papadantonakis et al., 2008).

Polyploidization or endoreplication is not only developmentally programmed, but is also an early step in the generation of aneuploid cancers. For instance, persistent DNA damage signals elicited by dysfunctional telomeres causes mitosis to be bypassed in p53-deficient cells (Davoli et al., 2010). Oscillations in ubiquitylation by the SCF^{Skp2} and APC^{Cdh1} complexes (Ang and Harper, 2004; Vodermaier, 2004; Nakayama and Nakayama, 2006) were observed during endoreplication in these cells using fluorescent ubiquitylation-based cell cycle indicator (Fucci) live-cell imaging.

[1]Lab for Cell Function Dynamics, BSI, RIKEN, 2-1 Hirosawa, Wako-city, Saitama 351-0198, Japan. [2]Life Function and Dynamics, ERATO, JST, 2-1 Hirosawa, Wako-city, Saitama 351-0198, Japan. [3]Subteam for Manipulation of Cell Fate, RIKEN BRC, 3-1-1 Koyadai, Tsukuba, Ibaraki 305-0074, Japan. [4]Research Resource Center, BSI, RIKEN, 2-1 Hirosawa, Wako-city, Saitama 351-0198, Japan.

*Author for correspondence (matsushi@brain.riken.jp)

Received 19 May 2013; Accepted 2 September 2013

Development (2013) doi:10.1242/dev.099226

Table 1. Summary of the Fucci transgenic mouse lines

Mouse lines	Features	References
mAG-hGem(1/110)*		
FucciS/G2/M-#504	Constant expression in most organs except hematopoietic system	Sakaue-Sawano et al., 2008; Stuckey et al., 2011; Hama et al., 2011; Ge et al., 2012
FucciS/G2/M-#492	Constant expression in hematopoietic organ; used for lymphatic studies	Aiba et al., 2010; Maruya et al., 2011; Kawamoto et al., 2012
FucciS/G2/M-#474	Constant expression in hematopoietic organ; used for HSC studies	This article
mKO2-hCdt1(30/120)*		
FucciG1-#596	Constant expression in most organs except hematopoietic system	Sakaue-Sawano et al., 2008; Juuri et al., 2012
FucciG1-#639	Constant expression in hematopoietic organ; used for lymphatic studies	Aiba et al., 2010
FucciG1-#610	Constant expression in hematopoietic organ; used for HSC studies	This article

*Under control of the CAGGS promoter.

This technology harnesses the cell cycle-dependent proteolysis of two ubiquitin oscillators, human CDT1 and geminin, which are the direct substrates of SCF^{Skp2} and APC^{Cdh1} complexes, respectively (Sakaue-Sawano et al., 2008). The Fucci probe consists of two chimeric proteins: mKO2 (monomeric Kusabira-Orange 2) fused to the ubiquitylation domain of CDT1 [FucciG1=mKO2-hCdt1(30/120)], which labels G1 phase nuclei red, and mAG (monomeric Azami-Green) fused to the ubiquitylation domain of geminin [FucciS/G2/M=mAG-hGem(1/110)], which labels S/G2/M phase nuclei green. We also observed that DNA damage-induced endoreplication occurs when normal murine mammary gland (NMuMG) cells were treated with etoposide, an inhibitor of DNA topoisomerase II (Sakaue-Sawano et al., 2011). The nuclei of NMuMG cells stably expressing Fucci probes changed from green to red without cell division and failed to exhibit any features consistent with mitosis, including nuclear envelope breakdown (NEB). Thus, Fucci probes can report reciprocal E3 ligase activities in DNA damage-induced endoreplication.

Regulation of ubiquitin oscillators by SCF^{Skp2} and APC^{Cdh1} complexes is crucial for normal development. *Cdh1*$^{-/-}$ embryos die at embryonic day (E) 9.5-10.5 owing to defects in endoreduplication of TSCs (García-Higuera et al., 2008; Li et al., 2008). Conversely, geminin$^{-/-}$ embryos fail to form an inner cell mass and exhibit premature endoreduplication at the eight-cell stage; as a result, all cells become committed to the trophoblast cell lineage (Gonzalez et al., 2006; Hara et al., 2006). In addition, early embryogenesis was examined using mice deficient in *Emi1*, which is known to be an APC/C inhibitor (Reimann et al., 2001). Although *Emi1*$^{-/-}$ embryos form polyploid TGCs, the inner cell mass does not develop properly, presumably because of the high degree of polyploidy and the abnormal cell-cycle progression (Lee et al., 2006). By contrast, Skp2 appears to be less crucial than Cdh1. *Skp2*$^{-/-}$ embryos are viable, but cells in knockout mice contain markedly enlarged nuclei with polyploidy and multiple centrosomes, resulting in reduced growth and increased apoptosis (Nakayama et al., 2000). However, these studies do not provide direct evidence that SCF^{Skp2} and APC^{Cdh1} activities oscillate reciprocally during the endoreduplication cycle.

Here, we used Fucci technology to study endoreplication in differentiating mouse TGCs and MKCs. To do this, we screened transgenic mouse lines expressing Fucci probes and identified mice that mark differentiating trophoblast cells and hematopoietic cells. We also designed special culture wells to track the cell cycle progression of cells isolated from these mice as they differentiated into TGCs or MKCs. Finally, we used the Sca*l*e technique, which renders fixed biological samples optically transparent, but preserves fluorescent signals in the clarified structures (Hama et al., 2011). By this technique, we were able to perform three-dimensional (3D) reconstruction of polyploid cells in whole placentas of transgenic pregnant mice. Using this combination of novel techniques, we show that TGCs and MKCs both skip cytokinesis, but using different mechanisms. In addition, we demonstrate that the transition from the SCF^{Skp2}- to APC^{Cdh1}-active state in differentiating MKCs varies with the polyploidy level.

RESULTS

Fucci transgenic mice

We previously generated eight transgenic mouse lines that constitutively express mAG-hGem(1/110) (FucciS/G2/M) and 16 lines constitutively expressing mKO2-hCdt1(30/120) (FucciG1) under the CAG promoter (Sakaue-Sawano et al., 2008). Our original work on the development of the Fucci technique used the FucciS/G2/M-#504 and FucciG1-#596 lines, which show nearly ubiquitous expression at early embryonic stages, with blastomere nuclei exhibiting green (FucciS/G2/M) or red (FucciG1) fluorescence (Table 1). Thus, to observe cell cycle changes during differentiation of trophoblast cells into TGCs, we cross-bred FucciS/G2/M-#504 and FucciG1-#596 mice and incubated blastocysts carrying both transgenes (#504/#596) in culture dishes.

For observation of MKC differentiation, these two lines were not suitable, as they did not show Fucci signals in the hematopoietic organs. We therefore performed extensive flow cytometry analysis using cell surface markers (Noda et al., 2008) to identify transgenic mouse lines expressing Fucci in the hematopoietic system. We found that FucciS/G2/M-#474 and FucciG1-#610 exhibited optimal signals in cells expressing a marker for cycling HSCs that have high repopulating activity (Table 1). We were therefore able to isolate HSCs from the bone marrow of the Fucci transgenic mice (#474/#610) and to observe cell cycle dynamics as they differentiated into MKCs.

Validation of Fucci performance during endoreplication

We first performed validation experiments using TGCs and MKCs isolated from #504/#596 and #474/#610 mice, respectively (supplementary material Fig. S1A-D), to demonstrate that the Fucci system can be used to study cell cycle regulation during endoreplication. Immediately after administration of 5-ethynyl-2′-deoxyuridine (EdU) to a pregnant mouse (#504/#596) for 20 minutes, E10.5 placental cells were isolated and subjected to the Click-iT reaction for labeling with Alexa 647 (supplementary material Fig. S1A). Bone marrow (BM) cells were isolated from a mouse (#474/#610), cultured in the presence of TPO for 7 days, treated with EdU for 20 minutes, and then subjected to the Click-iT reaction for labeling with Alexa 647 (supplementary material Fig. S1C). Prior to flow cytometric analysis, both samples were

Development (2013) doi:10.1242/dev.099226

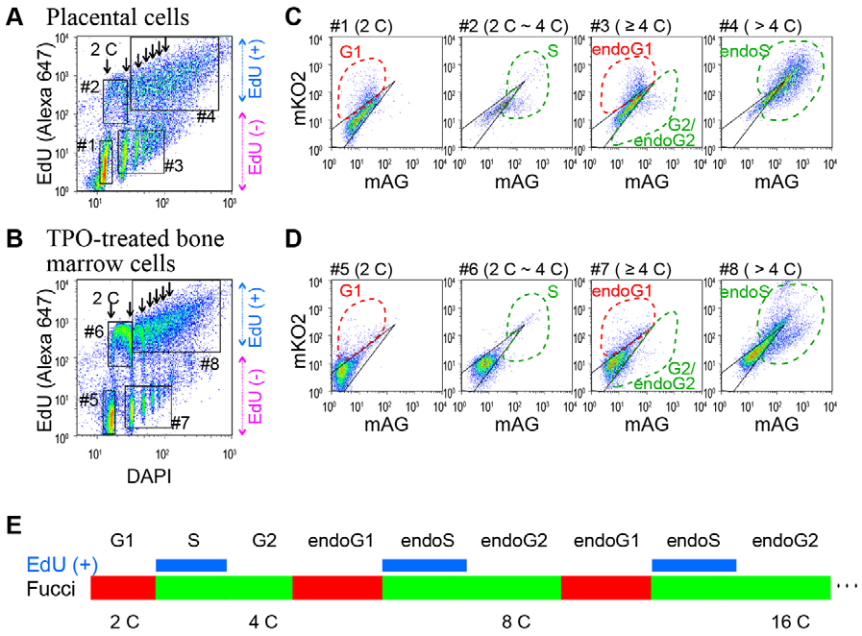

Fig. 1. Application of Fucci technology to analysis of endoreplicating cells. (A,B) Flow cytometry analysis of EdU incorporation (DNA synthesis) versus DAPI staining (DNA content) of placental cells from a #504/#596 mouse (A) and TPO-treated bone marrow cells from a #474/#610 mouse (B). Four cell fractions from each (#1-#4 in A; #5-#8 in B), which were characterized further, are indicated by boxes. (C,D) Flow cytometry analysis of Fucci signals (mKO2 versus mAG) of cells in fractions #1-#4 (C) and #5-#8 (D). Cells that are EdU(–), diploid (2 C) and mKO2(+) are assigned to cycling G1 (#1 and #5). Cells that are EdU(+), diploid ~tetraploid (2 C ~4 C) and mKO2(+)/mAG(+) or mAG(+) are assigned to S (#2 and #6). Cells that are EdU(–), polyploid (≥4 C) and mKO2(+) are assigned to endoG1 (#3 and #7). Cells that are EdU(–), polyploid (≥4 C) and mAG(+) are assigned to G2 or endoG2 (#3 and #7). Cells that are EdU(+), polyploid (>4 C) and mKO2(+)/mAG(+) or mAG(+) are assigned to endoS (#4 and #8). (E) The cell populations in terms of EdU incorporation, Fucci color and DNA content are schematized.

stained with 4′,6-diamidino-2-phenylindole (DAPI) (supplementary material Fig. S1B,D). Thus, all of the cells that transgenically exhibited the two-color fluorescence signals of Fucci probes produced fluorescence signals for the analysis of DNA synthesis (Alexa 647) and DNA content (DAPI). We performed multi-color flow cytometric analysis using four laser lines (supplementary material Fig. S2) to characterize polyploid populations in the samples. As cells in the cerebral cortex of an adult mouse are non-dividing diploid cells resting in G0/G1, they were used as the reference G0/G1 population (supplementary material Fig. S1E,F). Substantial DNA synthesis was detected in the placental and BM cell samples. Furthermore, prominent polyploidy associated with DNA synthesis was identified in both samples. By contrast, neither DNA synthesis nor polyploidization was found in the brain cell sample. Next, we obtained four fractions according to the EdU and DAPI signals for placental (Fig. 1A) and TPO-treated BM (Fig. 1B) cell samples each, and characterized their cell cycle phases (Fig. 1C,D, respectively). Fractions #1 and #5 produced an mKO2 signal and were supposed to represent the G1 population, whereas fractions #2 and #6 should represent the S population. Remarkably, by contrast, fractions #3, #4, #7 and #8 were composed of cells with ≥4 C. As illustrated in Fig. 1E, fractions #3 and #7 were EdU(–) and thus should consist of cells in the endoG1 and endoG2 populations (Hu and Cross, 2010) as well as the G2 population, whereas fractions #4 and #8 were EdU(+) and should represent the endoS population (Hu and Cross, 2010). These cell population data demonstrated that polyploid cells (>4 C) prepared from the Fucci transgenic mice had green or red nuclei according to cell cycle progression, which indeed involved DNA synthesis.

We also performed similar validation at the single-cell level. Another placenta from an EdU-administered pregnant mouse (#504/#596) was optically cleared using Sca*l*eA2 reagent (Hama et al., 2011) and then subjected to the Click-iT reaction and DAPI staining (Fig. 2). Multi-color imaging using a Zeiss LSM780 system with two-photon excitation and confocal configurations (supplementary material Fig. S2) allowed us to identify gigantic TGCs that carried EdU(–) red nuclei (endoG1), EdU(+) green nuclei (endoS) and EdU(–) green nuclei (endoG2).

Culture well for tracking all individual cells

During extended time-lapse imaging, target cells often migrate away from the field of view. To overcome this problem, we developed a culture well (FulTrac) with a poly(dimethylsiloxane) (PDMS) block stamped onto a glass coverslip (supplementary material Fig. S3). This allows us to fully track or trace individual cells as they progress through the cell cycle and differentiate. As the surface for cell growth is <0.33 mm in diameter, imaged cells remain inside the field of view of a 20× objective. Moreover, the FulTrac well has a stadium shape to maximize the numerical aperture (0.55) of the condenser for transmitted light. This enables high spatial resolution for differential interference contrast (DIC) imaging everywhere in the well, whereas conventional cylindrical wells give rise to shading in the periphery. For example, using an LCV100 microscope equipped with a FulTrac well, we were able to time-lapse image a morula-stage mouse embryo as it developed, all the way until it hatched from the zona pellucida (supplementary material Movie 1). Of particular importance is the design flexibility of FulTrac wells resulting from the ease of PDMS fabrication. For high-throughput analysis, we designed a PDMS block with four wells, performance of which can be maximized by a motorized microscope stage.

Visualizing endoreduplication of trophoblast cells

To visualize cell cycle dynamics in TGC development, we crossed a female FucciG1-#596 heterozygote to a male FucciS/G2/M-#504 homozygote and cultured individual blastocyst stage embryos in FulTrac wells. As was expected, half of the embryos carried both transgenes (#504/#596) and exhibited both green (FucciS/G2/M) and red (FucciG1) fluorescence. During incubation in KSOM-AA medium (Nishioka et al., 2008) for 1 day, most blastocysts completed hatching. Embryos were then subjected to long-term time-lapse imaging in RPMI1640 medium supplemented with 20% fetal bovine serum (FBS) (Fig. 3A). After a hatched blastocyst attached to the bottom surface of the well, cells in the trophectoderm layer migrated away from the inner cell mass (ICM) (Fig. 3B; supplementary material Movie 2). The nuclei of some cells switched between green and red (Fig. 3C), but no cellular features consistent with M phase, such as NEB, were ever observed during the color conversion. This is reminiscent of what was previously observed in

Development (2013) doi:10.1242/dev.099226

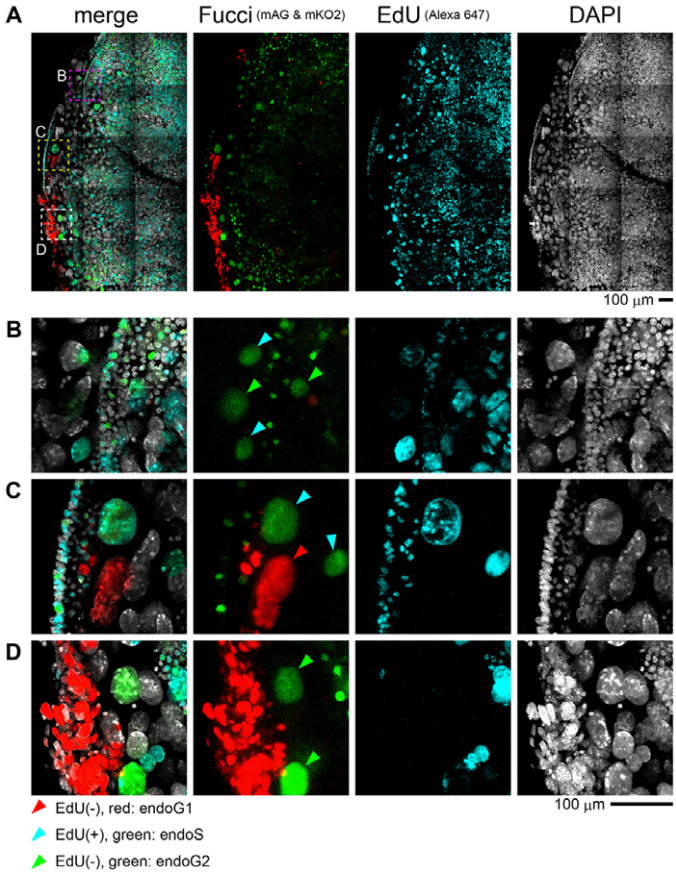

Fig. 2. Visualization of endoreduplicating cells within a whole placenta. Four-fluorophore imaging of endoreduplication in an optically cleared (Sca*l*eA2-treated) whole placenta (E10.5), which was prepared from a Fucci transgenic mouse (#504/#596) and stained for DNA synthesis [EdU (Alexa 647)] and DNA content (DAPI). Images were acquired using confocal (Fucci and EdU) or two-photon excitation (DAPI) microscopy. (A) Multiple images were combined using the microscope system's 'tiling' software. (B-D) Three regions (indicated by dashed boxes in A) in the periphery are enlarged. TGCs in endoG1 [EdU(–), red], endoS [EdU(+), green] and endoG2 [EdU(–), green] are indicated by red, cyan and green arrowheads, respectively.

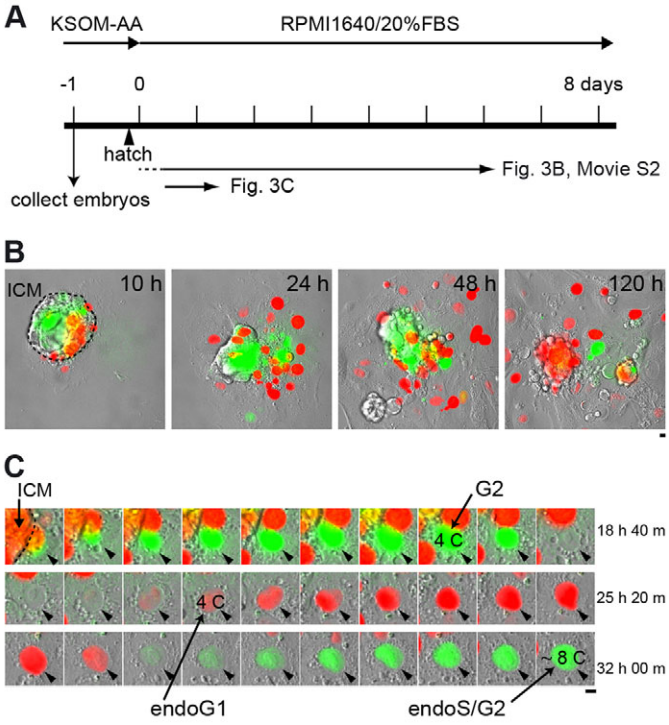

Fig. 3. Visualization of trophoblast endoreduplication in FulTrac wells by Fucci live-cell imaging. (A) A timetable of the preparation of blastocysts and time-lapse imaging. The endoreduplicative processes that were visualized in this study are indicated by solid lines. (B) Snapshots of trophoectoderm outgrowth from the ICM. (C) Endoreduplication of a mouse trophoblast giant cell with increasing chromatin ('C') values from 4 C to 8 C. C values denote DNA content as a multiple of the normal haploid genome. The Fucci fluorescence and DIC images were merged. Arrowheads indicate an endoreduplicating trophoblast cell. Scale bars: 10 μm.

etoposide-treated NMuMG cells (supplementary material Fig. S4) (Sakaue-Sawano et al., 2011). These endoreduplicating cells eventually exhibited large, red (endoG1) or green (endoS/G2) nuclei and were morphologically identifiable as differentiated, polyploid TGCs (Fig. 3B, 120 hours). By reliably tracking individual cells on the ICM with 40-minute intervals (Fig. 3C), we were able to identify mitotic, diploid trophoblast cells (black arrowheads), which then differentiated into polyploid TGCs, and to assign chromatin (C) values to individual cells across time.

To gain a comprehensive 3D perspective of the endoreduplication cycle in TGCs, we examined Fucci signals in optically cleared placentas of #504/#596 embryos. Placentas with intact maternal decidua tissues at various gestation stages were treated with Sca*l*eU2 (Hama et al., 2011) for >2 months. We imaged a whole E10.5 sample from the embryonic side (Fig. 4A). We used a confocal microscopy system (FV1000) equipped with a 40× silicone-oil objective to acquire high-resolution images of Fucci signals residing deep inside the sample and verified their nuclear localization by DAPI staining (Fig. 4B). Next, using a macro-confocal microscopy system (AZ-C1) equipped with a 2× objective, we obtained a 2D projection image of the entire placenta (Fig. 4C). Then we substituted a 4× objective for higher magnification views in central (Fig. 4D-H) and peripheral (Fig. 4I-M) regions of the placenta. Highly polyploid TGCs with giant nuclei (>100 μm in diameter) were located peripherally at a depth of 0.6-1.0 mm, in the junctional zone (Fig. 4J-L). At this stage (E10.5), the green (endoS/G2) and red (endoG1) giant nuclei were observed in equal proportion. As their distributions appeared to be random, it is likely that no intercellular or spatial regulation governs progression of the endoreduplication cycle. By contrast, the central region was abundant with green and red nuclei of normal size (~10 μm in diameter), which might belong to diploid spongiotrophoblast (SpT) cells or less differentiated TGCs. The lack of highly polyploid TGCs in the central region was confirmed by 3D reconstruction experiments using two other E10.5 samples. These results suggest a centripetal pattern of differentiation of TGCs in the placenta. Highly polyploid TGCs with nuclear size >150,000 μm^3 were automatically identified using commercial software (Volocity) in the peripheral regions of transparent placentas prepared at E8.5, E9.5, E10.5, E11.5, E12.5 and E13.5 (supplementary material Fig. S5). Their number increased drastically between E9.5 and E10.5, and then the ratio of the green (endoS/G2) to red (endoG1) nuclei decreased. By E13.5, >99% of the gigantic cells had red (endoG1) nuclei. Thus, endoreduplicative cycling appears to be almost complete by E13.5 and produces terminally differentiated TGCs.

Visualizing endomitosis of MKBs and MKCs

To monitor endomitosis in HSCs as they differentiate into MKCs, we used two transgenic lines that mark hematopoietic cell nuclei

Development (2013) doi:10.1242/dev.099226

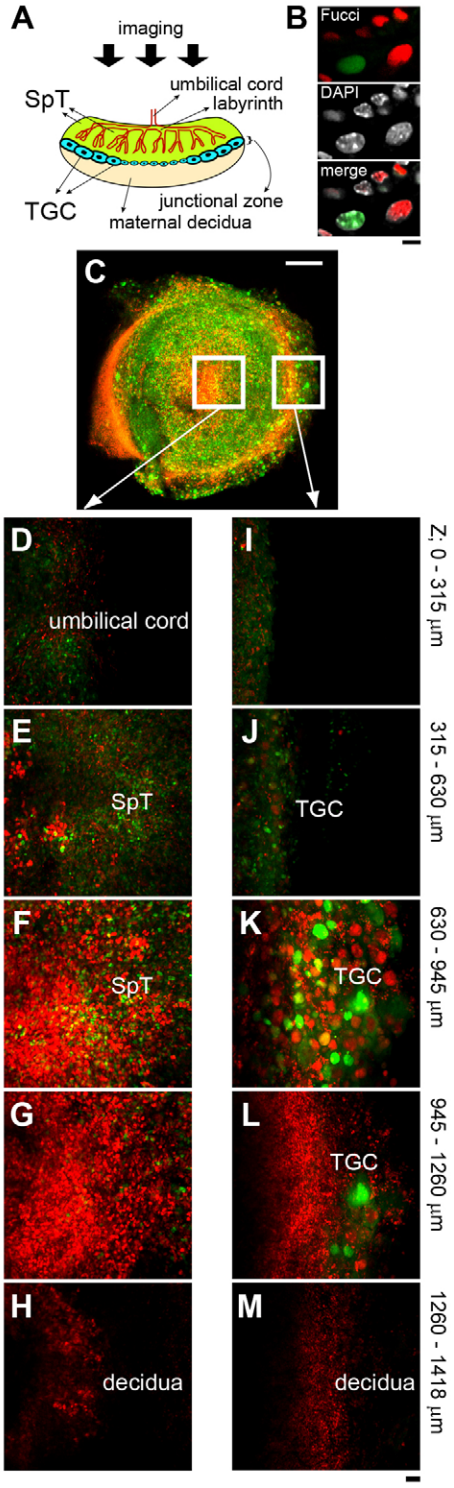

Fig. 4. Three-dimensional reconstructions of a Fucci-expressing mouse placenta. (A) Schematic of an E10.5 mouse conceptus.Tissue was fixed with 4% PFA and treated with Sca*l*eU2 for 2 months. (B) High-resolution confocal images of giant nuclei labeled with Fucci and DAPI inside the placenta (#504/#596). Unsectioned tissue was imaged using a confocal microscope. (C) A projection image of Fucci-labeled nuclei in the placenta (#504/#596) and the maternal decidua (#596). Unsectioned tissue was imaged using a macro-zoom confocal microscope. (D-H) Five consecutive projection images of the center region (left white box in C). Each projection image consisted of 100 confocal images and spanned 315 µm along the *z*-axis. (I-M) Five consecutive projection images of the peripheral region (right white box in C). Scale bars: 10 µm (B); 1 mm (C); 100 µm (D-M).

with green (FucciS/G2/M-#474) and red (FucciG1-#610) fluorescence (Table 1; Fig. 5). $CD34^{-}$/c-Kit^{+}/$Sca\text{-}1^{+}$/Lin^{-} cells (HSCs) were isolated from the bone marrow of adult #474/#610 mice and were used for further studies (supplementary material Fig. S6A). First, we analyzed the fluorescence intensities of mKO2 (red) and mAG (green) of these HSC, multipotent progenitor (MPP), mature B and immature B cell fractions by flow cytometry (supplementary material Fig. S6B). In each fraction, we identified two cell populations with high and low intensities of mKO2 signals for CDT1 accumulation, which we hypothesize correspond to quiescent G0 and cycling G1 cells, respectively. Because the HSCs exhibited a high intensity of mKO2 (red) fluorescence (supplementary material Fig. S6B, HSC), the #474/#610-derived HSC fraction was assumed to be enriched with quiescent G0 cells. We transferred the HSCs into the FulTrac well with a medium containing TPO (Fig. 5A). Nearly all of the cell nuclei were red (G0) in the beginning, but turned green (S/G2/M) after ~2 days, as revealed by the time-lapse imaging (supplementary material Fig. S7 and Movie 3). This slow proliferation switch in HSCs is corroborated by previous bromodeoxyuridine (BrdU) incorporation analyses (Passegué et al., 2005). After re-entering the cell cycle, some cells switch to an endomitotic cell cycle. At DIV (days *in vitro*) 8, giant cells with green (endoS/G2) or red (endoG1) nuclei appeared (Fig. 5B, HSC, DIV 8), which we assumed to be highly polyploid megakaryoblasts (supplementary material Fig. S8). These cell nuclei alternated between green and red multiple times as they grew and differentiated. The cells finally became presumptive MKCs with red nuclei.

Using combinations of cell surface markers, we isolated MPPs, common myeloid progenitors (CMPs), megakaryocyte-erythroid progenitors (MEPs) and MKCs (supplementary material Fig. S6A). They were kept in FulTrac wells for time-lapse imaging (Fig. 5B; supplementary material Fig. S6C). We observed endomitosing megakaryoblasts in MPP, CMP and MEP cultures. In the MKC culture, we observed mature MKCs with red nuclei exhibiting hallmark features of proplatelets (supplementary material Fig. S6C, arrowhead) (Patel et al., 2005).

We also examined nuclear structures during endomitosis in MKCs (Fig. 5C). The green-to-red conversion (the endoG2/endoG1 transition) was accompanied by breakdown of the nuclear envelope, consistent with the fact that polyploidy in MKCs is achieved via endomitosis. Interestingly, upon the disappearance of the green fluorescence, cells rapidly adhered to the coverslip and then gradually returned to spheres. This transient morphological change was easily quantified by measuring the cell diameter (Fig. 5D). We were also able to determine the C values of individual differentiating cells and observed that nuclei spent a longer time in the green (endoS/G2) or red (endoG1) state as polyploidy increased (supplementary material Fig. S9 and Movie 4). During the green-to-red conversion, in particular, the latency time for the emergence of the red signal (endoG1 entry) was longer in highly polyploid cells (≥16 C) (supplementary material Fig. S10).

Comparison of endoreplication in TGCs and MKCs

Although APC^{Cdh1} is activated at the metaphase/anaphase transition in the mitotic cell cycle, it also functions at the endoG2/endoG1 transition in TGC endoreduplication and MKC endomitosis. However, cellular features consistent with M phase were observed, including NEB, during the endoG2/endoG1 transition of MKCs but not TGCs (Fig. 6A). We detailed the temporal profiles of the transition in multiple cells and attempted to superimpose them (Fig. 6B-D). In TGCs, the rate at which the green fluorescence

Development (2013) doi:10.1242/dev.099226

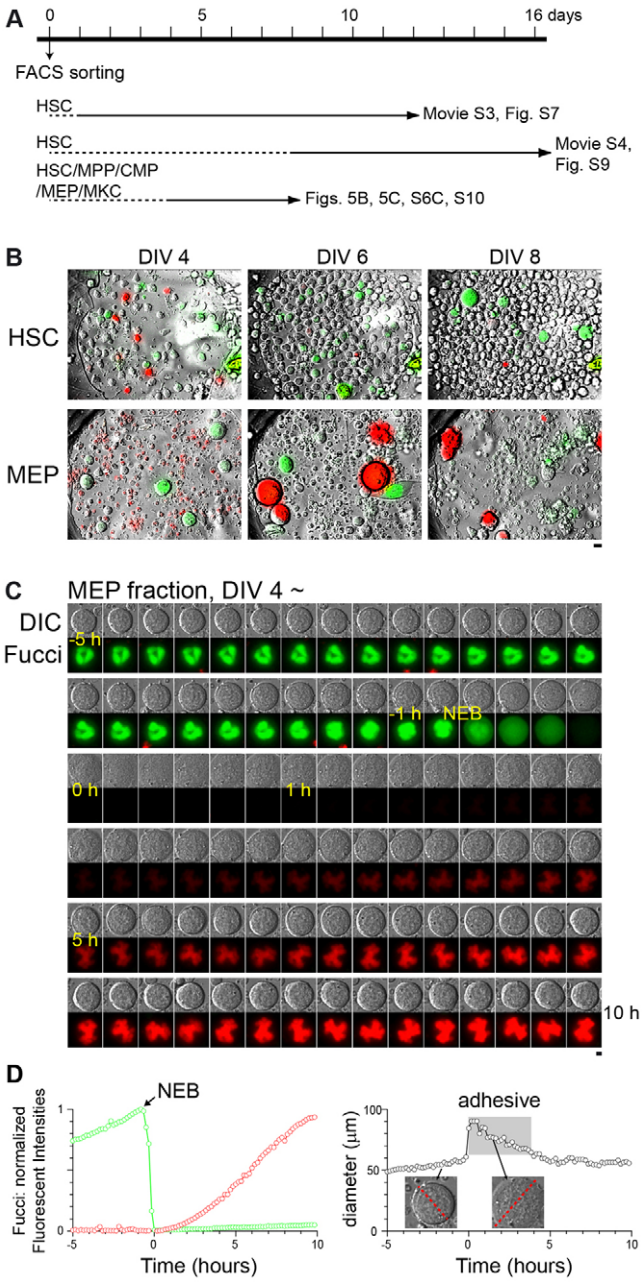

Fig. 5. Visualization of MKB endomitosis in FulTrac wells by Fucci live-cell imaging. (A) A timetable of the preparation of cell fractions and time-lapse imaging. The endomitotic processes that were visualized in this study are indicated by solid lines. (B) Typical fluorescence and DIC images of Fucci-expressing cells at DIV 4, 6 and 8 originating in HSC and MEP fractions. (C) Endomitosis tracking of a cell derived from the MEP fraction during a green-to-red conversion. A series of DIC (top) and Fucci fluorescence (bottom) images later than DIV 4. (D) Temporal profiles of fluorescence intensities of mAG-hGem(1/110) (green line) and mKO2-hCdt1(30/120) (red line) (left) and morphology (right) tracked from images shown in C images. NEB was identified by the abrupt spread of Fucci green fluorescence over the entire cell (Leung et al., 2004). Scale bars: 10 µm.

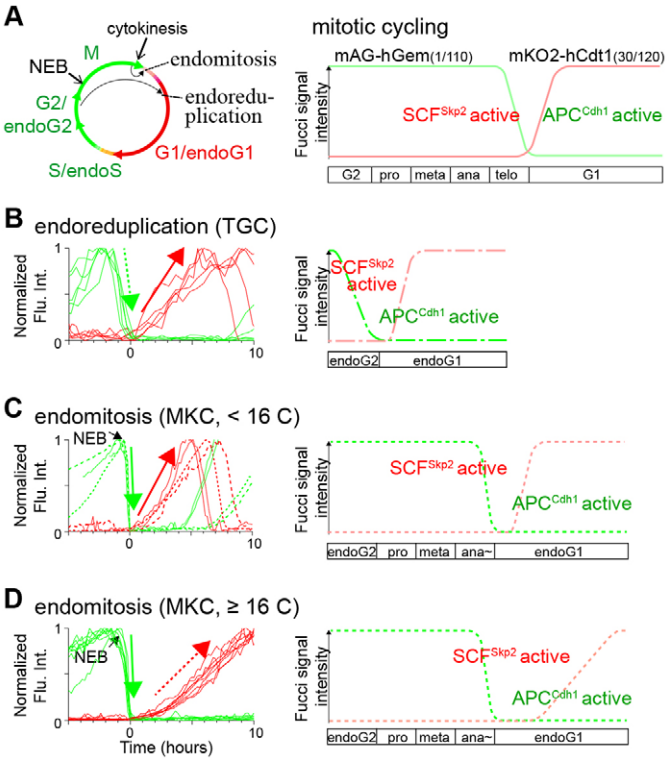

Fig. 6. Endoreduplication and endomitosis bypass aspects of mitosis to different extents. (A) The generic mitotic cell cycle is indicated by the round circle. The cell cycle phases bypassed in TGCs and MKBs are indicated by black arrows. (B-D) Observed Fucci signals during green-to-red conversions (transitions from endoG2 to endoG1) in TGCs (B), and low ploidy (<16 C) (C) and high ploidy (≥16 C) (D) differentiating MKBs. Temporal profiles of fluorescence intensities of mAG-hGem(1/110) and mKO2-hCdt1(30/120) are indicated by green and red lines, respectively. The ubiquitin oscillators composed of SCF^{Skp2} and APC^{Cdh1} maintain the bistability at the direct transition from endoG2 to endoG1 in endoreduplication or at the endoG2/endoG1 transition through the abortive M phase in endomitosis.

disappeared and the red fluorescence appeared was constant, irrespective of polyploidy level (Fig. 6B). By contrast, the polyploidy of MKCs determined the speed of green-to-red conversion (endoG2/endoG1 transition). In low polyploidy MKCs (<16 C), the emergence and subsequent extinction of red fluorescence (endoG1 entry and exit) was variable but rapid (Fig. 6C), whereas the appearance of red fluorescence (endoG1 entry) in high polyploidy MKCs (≥16 C) was consistently slow (Fig. 6D; supplementary material Fig. S10). To summarize, green-to-red conversions of Fucci signals during mitotic cycling, endoreduplication and endomitosis are illustrated with respect to the normal cell cycle phases, from G2 to G1 to M (Fig. 6).

DISCUSSION

Visualizing the cell cycle behavior of individual cells within complex tissues has in the past been extremely difficult. For instance, it has not been clear whether the ubiquitin oscillators that control normal mitotic cell cycle transitions (Ang and Harper, 2004; Vodermaier, 2004; Nakayama and Nakayama, 2006) function during endoreplication. Previous work showed that the protein level of the cyclin-dependent kinase inhibitor p57 (also known as Cdkn1c), which is targeted by SCF^{Skp2} for degradation, oscillates in endoreduplicating mammalian cells (TGCs) in culture (Hattori et al., 2000; Ullah et al., 2008). Because the promoter activity of p57 is constant in TGCs, it was surmised that the enzymatic activity of SCF^{Skp2} must oscillate. In endoreplicating *Drosophila* cells, oscillation in $APC^{Fzr/Cdh1}$ activity was verified by measuring the protein level of its substrate, Origin recognition complex 1 (Orc1) (Asano and Wharton, 1999; Narbonne-Reveau et al., 2008). Although these findings support the function of

Development (2013) doi:10.1242/dev.099226

ubiquitin oscillators in endoreplicative cycling, most of the data are snapshots correlating substrate expression levels and S phase markers, such as BrdU incorporation. Importantly, in addition, none of these studies examined both APC^{Cdh1} and SCF^{Skp2} activities at the same time. Thus, little was known about the precise timing of the transitions between the APC^{Cdh1}- and SCF^{Skp2}-active states during endoreplicative cycles. A recent computational study simulated the oscillatory dynamics of the $APC^{Fzr/Cdh1}$ and $CRL4^{CDT2}$ ubiquitin ligases in endoreplicating *Drosophila* cells (Zielke et al., 2011).

In the present study, we overcame previous limitations by performing live imaging of TGCs and MKCs using Fucci probes. This allowed us to monitor the anti-phase oscillating activities of the two E3 ligases, with high contrast and high temporal resolution. In particular, our *ex vivo* imaging using custom FulTrac wells permitted us to observe individual cells over a long time period. This work lays the foundation for future studies of endoreduplication and endomitosis in a multicellular context; for example, in living intact placenta and bone marrow. This is important because the endoreplicative cell cycle is regulated not only by intracellular signals but also by extracellular signals, although a recent integrative model for the cyclin/Cdk network in mammalian endoreplicative cells suggests that it functions as a self-sustained oscillator (Gérard and Goldbeter, 2009).

The temporal profiles of the green-to-red conversion of Fucci signals (Fig. 6) might yield clues as to what activates APC^{Cdh1} during endoG2 phase or abortive mitosis. It is thus interesting to investigate temporal patterns of the activation of APC^{Cdh1} regulators, such as Emi1. Furthermore, the reciprocal activation of SCF^{Skp2} and APC^{Cdh1} is modified during differentiation into MKCs. The relatively slow conversion seen in high-polyploidy (≥16 C) MKCs suggests the existence of a state in which APC^{Cdh1} is fully activated whereas SCF^{Skp2} is not yet fully inactivated. Although the APC^{Cdh1} complex directly targets the SCF^{Skp2} complex for degradation and vice versa, there might be other mechanisms that regulate the anti-phase oscillation between the two E3 ligase activities. Notably, similar ploidy-level dependence was observed for the differential downregulation of two guanine nucleotide exchange factors [GEF-H1 (also known as Arhgef2) and ECT2] in endomitosing MKCs (Gao et al., 2012).

The Fucci transgenic mouse lines we have generated will be very useful for a variety of future studies. Crossing Fucci lines to the many mutant lines isolated by forward genetic screens will allow identification of the molecules responsible for the initiation, progression and termination of endoreplication. This information will refine computational models, which attempt to account for mammalian endoreplication. Also, crossing Fucci mice to the numerous transgenic lines expressing fluorescent markers under the control of cell type- or stage-specific promoters will be fruitful. Finally, Fucci transgenic mice will help researchers to re-evaluate polyploidy in cell types other than TGCs and MKCs. For example, the presence of polyploid neurons in vertebrates has been debated for the last half century; tetraploidy has been described in retinal ganglion cells (Morillo et al., 2010), cerebellar Purkinje neurons (Das, 1977) and cortical neurons of Alzheimer's disease patients (Mosch et al., 2007). In addition, an intriguing attempt would be the three-dimensional reconstructions of Fucci-labeled hepatocytes in the developing or regenerating liver, because hepatocytes show unique polyploidization (Duncan et al., 2010).

MATERIALS AND METHODS

Fucci transgenic mice

Fucci transgenic mice were generated by expressing mAG-hGem(1/110) [DDBJ/EMBL/GenBank, AB370333] (FucciS/G2/M) or mKO2-hCdt1(30/120) [DDBJ/EMBL/GenBank, AB370332] (FucciG1) under the control of the CAGGS promoter (Sakaue-Sawano et al., 2008). Transgenic mouse lines FucciS/G2/M-#474, -#492 or -#504, and FucciG1-#596, -#610 or -#639 along with genotyping protocols can be obtained from the RIKEN Bio Resource Center (BRC) website http://www.brc.riken.jp/lab/animal/en/. The experimental procedures and housing conditions for the animals were approved by the Animal Experimental Committees at the Institute of Physical and Chemical Research (RIKEN) – Brain Science Institute (BSI) and Bio Resource Center (BRC) – and all animals were cared for and treated humanely in accordance with the Institutional Guidelines for Experiments using Animals.

FulTrac

PDMS-based devices (FulTrac) were constructed as described previously (Hirano et al., 2010).

Cell cycle analysis of endoreplicating cells

Pregnant mice were injected intravenously with EdU solution (Life Technologies) (50 mg/kg body weight). After 20 minutes, placentas at E10.5 were removed, minced, and dissociated with 500 U/ml collagenase I (Worthington) at 37°C for 30 minutes and then with 6.25 U/ml DNase I (Worthington) for 30 minutes. After being washed and passed through a 100-μm nylon mesh, the placental cells were fixed with 4% paraformaldehyde (PFA) for 10 minutes on ice. The fixed cells were treated with azide-conjugated Alexa 647 by the Click-iT reaction (Life Technologies) with slight modification. As copper ion used for the conjugation between EdU and Alexa dyes in the Click-iT reaction tended to quench fluorescent proteins, we attempted to lower the copper ion concentration. We found that one-third of the copper ion concentration recommended by the manufacturer was sufficient for the reaction while effectively avoiding the quenching reaction. Finally, the cell samples were stained with 3 μM DAPI and analyzed using a FACSAria II (BD Biosciences). DAPI was excited by a 355-nm laser line and its emission collected through 450/50BP; mAG was excited by a 488-nm laser line and its emission collected through 530/30BP; mKO2 was excited by a 561-nm laser line and its emission collected through 610/20BP; and Alexa 647 was excited by a 640-nm laser line and its emission collected through 710/50BP. The data were analyzed using FlowJo software (Tree Star).

Mouse bone marrow cells were cultured for 7 days with DMEM/F12 supplemented with 5% FBS, 10 ng/ml mouse stem cell factor (Peprotech), 100 ng/ml human thrombopoietin (TPO) (Peprotech), 10 ng/ml mouse Fgf1 (Invitrogen), and 20 ng/ml mouse insulin-like growth factor 2 (Igf2) (R&D Systems). The cells were treated with 100 μM EdU for 20 minutes and the Click-iT reaction was subsequently performed as for placental cells.

LCV100 microscopy

Cells were subjected to long-term, time-lapse imaging using a computer-assisted fluorescence microscope (Olympus, LCV100) equipped with an objective lens (Olympus, UAPO 40×/340 N.A.=0.90), a 0.5×zoom lens, a halogen lamp, a red light emitting diode (LED) (620 nm), a charge coupled device camera (Olympus, DP30), DIC optical components, and interference filters. The halogen lamp was used with a 470DF35 excitation filter, a 505DRLP dichroic mirror and a 510WB40 emission filter to observe the mAG fluorescence, and a BP520-540HQ excitation filter, a DM545HQ dichroic mirror and a BP555-600HQ emission filter to observe the mKO2 fluorescence. For DIC imaging, the red LED was used with a filter cube containing an analyzer. Image acquisition and analysis were performed using MetaMorph 6.37 and 7.6.0.0 software (Universal Imaging Corporation), respectively.

Time-lapse imaging of trophoblast cell endoreduplication

FucciG1-#596 heterozygous eggs and FucciS/G2/M-#504 homozygous sperm were used for *in vitro* fertilization. Fertilized eggs were cultured to the two-cell stage and then were frozen as stocks. After thawing, two-cell stage embryos were transplanted into pseudopregnant female mice. After 3 days, blastocysts were collected from the uterus, and were individually cultured in FulTrac wells in KSOM-AA medium for 24 hours in a CO_2

incubator. Then, the medium was changed to RPMI1640 containing 20% fetal calf serum. Trophoectoderm outgrowth from the inner cell mass was time-lapse imaged using an LCV100 microscope.

Whole-placenta imaging

FucciS/G2/M-#504 and FucciG1-#596 mice were cross-bred and placentas were excised at E8.5, E9.5, E10.5, E11.5, E12.5 and E13.5 and fixed with 4% PFA. Tissue was cryoprotected in PBS containing 20% sucrose, and optically cleared with Sca*l*eU2 solution (4 M urea, 30% glycerol and 0.1% Triton X-100) (Hama et al., 2011). Cleared placentas were embedded in a Sca*l*eU2-soaked gel. Whole-placenta imaging was performed using an AZ-C1 macro-zoom confocal microscope (Nikon) equipped with 488 nm and 561 nm laser lines, an AZ-Plan Fluor 2×objective lens (N.A.=0.2, W.D.=45 mm), or an AZ-Plan Apo 4×objective lens (N.A.=0.4, W.D.=20 mm). Confocal images were taken every 315 µm along the *z*-axis to create *z* stacks. Also, a fixed #504/#596 placenta at E10.5, which had been labeled with EdU (Alexa 647) and DAPI, was imaged using an Olympus FV1000 confocal microscope equipped with a UPLSAPO 40×silicone-oil objective lens (N.A.=1.25, W.D.=0.3 mm) or a Zeiss LSM 780 confocal/multiphoton microscope equipped with a W Plan-Apochromat 20×objective lens (N.A.=1.0, W.D.=1.9 mm). The DAPI dye was excited by a 405-nm laser line (FV1000) or two-photon excitation at 780 nm (LSM 780).

Fractionation of blood cells

Cell fractionation was carried out as described previously (Noda et al., 2008). Briefly, blood cells isolated from Fucci transgenic mice (#474/#610) (6-7 months old) were stained with cell surface markers and sorted using a FACS Vantage SE (BD Biosciences). Fractionated cells were cultured in FulTrac wells containing DMEM/F12 supplemented with 10 ng/ml mouse stem cell factor (Peprotech), 100 ng/ml human thrombopoietin (TPO) (Peprotech), 10 ng/ml mouse Fgf1 (Invitrogen) and 20 ng/ml mouse insulin-like growth factor 2 (Igf2) (R&D Systems).

Time-lapse imaging of megakaryocyte endomitosis

Bone marrow cells were isolated from an adult Fucci transgenic mouse (#474/#610), and hematopoietic stem cells [CD34(–)/c-kit(+)/Sca1(+)/lineage(–)] were purified using flow cytometry (Noda et al., 2008). The cells were cultured in the FulTrac wells under conditions that promote differentiation into megakaryocytes, and were time-lapse imaged using an LCV100 microscope.

Estimation of ploidy level

In this study, we determined the ploidy (the C value) for some TGCs and MKCs cultured in FulTrac wells, which enabled full tracking of individual cells over an extended period. We traced TGCs and MKCs back to cells inside the ICM and cells before exposure to TPO, respectively. These original cells had not entered the endoreplicative cell cycle yet and were supposed to be in the normal mitotic cell cycle (2 C ~4 C).

Acknowledgements

We thank H. Hama, T. Watanabe, K. Hosoya and N. Ito for technical assistance and discussion.

Competing interests

The authors declare no competing financial interests.

Author contributions

A.S.-S., E.T., H.M. and A.M. conceived and designed the study. A.S.-S., T.H., M.Y., R.T., K.O., T.A. and S.N. carried out the experiments. A.S.-S., M.Y. and S.N. analyzed the data. A.S.-S. and A.M. prepared the manuscript. A.M. supervised the project.

Funding

This work was partly supported by Grants-in-Aid for Scientific Research on Innovative Areas ‘Fluorescence Live imaging’ and ‘Cell Fate’ from The Ministry of Education, Culture, Sports, Science, and Technology, Japan (Japan MEXT); and a Grant-in-Aid for challenging Exploratory Research, Research Program of Innovative Cell Biology from Innovative Technology (Cell Innovation). Deposited in PMC for immediate release.

Supplementary material

Supplementary material available online at
http://dev.biologists.org/lookup/suppl/doi:10.1242/dev.099226/-/DC1

References

Aiba, Y., Kometani, K., Hamadate, M., Moriyama, S., Sakaue-Sawano, A., Tomura, M., Luche, H., Fehling, H. J., Casellas, R., Kanagawa, O. et al. (2010). Preferential localization of IgG memory B cells adjacent to contracted germinal centers. *Proc. Natl. Acad. Sci. USA* **107**, 12192-12197.

Ang, X. L. and Harper, J. W. (2004). Interwoven ubiquitination oscillators and control of cell cycle transitions. *Sci. STKE* **2004**, pe31.

Asano, M. and Wharton, R. P. (1999). E2F mediates developmental and cell cycle regulation of ORC1 in Drosophila. *EMBO J.* **18**, 2435-2448.

Bermejo, R., Vilaboa, N. and Calés, C. (2002). Regulation of CDC6, geminin, and CDT1 in human cells that undergo polyploidization. *Mol. Biol. Cell* **13**, 3989-4000.

Carow, C. E., Fox, N. E. and Kaushansky, K. (2001). Kinetics of endomitosis in primary murine megakaryocytes. *J. Cell. Physiol.* **188**, 291-303.

Chen, H. Z., Ouseph, M. M., Li, J., Pécot, T., Chokshi, V., Kent, L., Bae, S., Byrne, M., Duran, C., Comstock, G. et al. (2012). Canonical and atypical E2Fs regulate the mammalian endocycle. *Nat. Cell Biol.* **14**, 1192-1202.

Das, G. D. (1977). Induction of mitosis in the differentiating Purkinje cells of the cerebellum. *Acta Anat. (Basel)* **97**, 435-442.

Davoli, T. and de Lange, T. (2011). The causes and consequences of polyploidy in normal development and cancer. *Annu. Rev. Cell Dev. Biol.* **27**, 585-610.

Davoli, T., Denchi, E. L. and de Lange, T. (2010). Persistent telomere damage induces bypass of mitosis and tetraploidy. *Cell* **141**, 81-93.

Duncan, A. W., Taylor, M. H., Hickey, R. D., Hanlon Newell, A. E., Lenzi, M. L., Olson, S. B., Finegold, M. J. and Grompe, M. (2010). The ploidy conveyor of mature hepatocytes as a source of genetic variation. *Nature* **467**, 707-710.

Edgar, B. A. and Orr-Weaver, T. L. (2001). Endoreplication cell cycles: more for less. *Cell* **105**, 297-306.

Eliades, A., Papadantonakis, N. and Ravid, K. (2010). New roles for cyclin E in megakaryocytic polyploidization. *J. Biol. Chem.* **285**, 18909-18917.

Gao, Y., Smith, E., Ker, E., Campbell, P., Cheng, E. C., Zou, S., Lin, S., Wang, L., Halene, S. and Krause, D. S. (2012). Role of RhoA-specific guanine exchange factors in regulation of endomitosis in megakaryocytes. *Dev. Cell* **22**, 573-584.

García-Higuera, I., Manchado, E., Dubus, P., Cañamero, M., Méndez, J., Moreno, S. and Malumbres, M. (2008). Genomic stability and tumour suppression by the APC/C cofactor Cdh1. *Nat. Cell Biol.* **10**, 802-811.

Ge, W. P., Miyawaki, A., Gage, F. H., Jan, Y. N. and Jan, L. Y. (2012). Local generation of glia is a major astrocyte source in postnatal cortex. *Nature* **484**, 376-380.

Geddis, A. E., Fox, N. E., Tkachenko, E. and Kaushansky, K. (2007). Endomitotic megakaryocytes that form a bipolar spindle exhibit cleavage furrow ingression followed by furrow regression. *Cell Cycle* **6**, 455-460.

Gérard, C. and Goldbeter, A. (2009). Temporal self-organization of the cyclin/Cdk network driving the mammalian cell cycle. *Proc. Natl. Acad. Sci. USA* **106**, 21643-21648.

Gonzalez, M. A., Tachibana, K. E., Adams, D. J., van der Weyden, L., Hemberger, M., Coleman, N., Bradley, A. and Laskey, R. A. (2006). Geminin is essential to prevent endoreduplication and to form pluripotent cells during mammalian development. *Genes Dev.* **20**, 1880-1884.

Hama, H., Kurokawa, H., Kawano, H., Ando, R., Shimogori, T., Noda, H., Fukami, K., Sakaue-Sawano, A. and Miyawaki, A. (2011). Scale: a chemical approach for fluorescence imaging and reconstruction of transparent mouse brain. *Nat. Neurosci.* **14**, 1481-1488.

Hara, K., Nakayama, K. I. and Nakayama, K. (2006). Geminin is essential for the development of preimplantation mouse embryos. *Genes Cells* **11**, 1281-1293.

Hattori, N., Davies, T. C., Anson-Cartwright, L. and Cross, J. C. (2000). Periodic expression of the cyclin-dependent kinase inhibitor p57(Kip2) in trophoblast giant cells defines a G2-like gap phase of the endocycle. *Mol. Biol. Cell* **11**, 1037-1045.

Hirano, M., Hoshida, T., Sakaue-Sawano, A. and Miyawaki, A. (2010). A poly(dimethylsiloxane)-based device enabling time-lapse imaging with high spatial resolution. *Biochem. Biophys. Res. Commun.* **392**, 307-310.

Hu, D. and Cross, J. C. (2010). Development and function of trophoblast giant cells in the rodent placenta. *Int. J. Dev. Biol.* **54**, 341-354.

Juuri, E., Saito, K., Ahtiainen, L., Seidel, K., Tummers, M., Hochedlinger, K., Klein, O. D., Thesleff, I. and Michon, F. (2012). Sox2+ stem cells contribute to all epithelial lineages of the tooth via Sfrp5+ progenitors. *Dev. Cell* **23**, 317-328.

Kawamoto, S., Tran, T. H., Maruya, M., Suzuki, K., Doi, Y., Tsutsui, Y., Kato, L. M. and Fagarasan, S. (2012). The inhibitory receptor PD-1 regulates IgA selection and bacterial composition in the gut. *Science* **336**, 485-489.

Lammens, T., Boudolf, V., Kheibarshekan, L., Zalmas, L. P., Gaamouche, T., Maes, S., Vanstraelen, M., Kondorosi, E., La Thangue, N. B., Govaerts, W. et al. (2008). Atypical E2F activity restrains APC/CCCS52A2 function obligatory for endocycle onset. *Proc. Natl. Acad. Sci. USA* **105**, 14721-14726.

Lee, H., Lee, D. J., Oh, S. P., Park, H. D., Nam, H. H., Kim, J. M. and Lim, D. S. (2006). Mouse emi1 has an essential function in mitotic progression during early embryogenesis. *Mol. Cell. Biol.* **26**, 5373-5381.

Lee, H. O., Davidson, J. M. and Duronio, R. J. (2009). Endoreplication: polyploidy with purpose. *Genes Dev.* **23**, 2461-2477.

Leung, A. K., Gerlich, D., Miller, G., Lyon, C., Lam, Y. W., Lleres, D., Daigle, N., Zomerdijk, J., Ellenberg, J. and Lamond, A. I. (2004). Quantitative kinetic analysis

of nucleolar breakdown and reassembly during mitosis in live human cells. *J. Cell Biol.* **166**, 787-800.
Li, M., Shin, Y. H., Hou, L., Huang, X., Wei, Z., Klann, E. and Zhang, P. (2008). The adaptor protein of the anaphase promoting complex Cdh1 is essential in maintaining replicative lifespan and in learning and memory. *Nat. Cell Biol.* **10**, 1083-1089.
Martindill, D. M. and Riley, P. R. (2008). Cell cycle switch to endocycle: the nucleolus lends a hand. *Cell Cycle* **7**, 17-23.
Maruya, M., Suzuki, K., Fujimoto, H., Miyajima, M., Kanagawa, O., Wakayama, T. and Fagarasan, S. (2011). Vitamin A-dependent transcriptional activation of the nuclear factor of activated T cells c1 (NFATc1) is critical for the development and survival of B1 cells. *Proc. Natl. Acad. Sci. USA* **108**, 722-727.
Morillo, S. M., Escoll, P., de la Hera, A. and Frade, J. M. (2010). Somatic tetraploidy in specific chick retinal ganglion cells induced by nerve growth factor. *Proc. Natl. Acad. Sci. USA* **107**, 109-114.
Mosch, B., Morawski, M., Mittag, A., Lenz, D., Tarnok, A. and Arendt, T. (2007). Aneuploidy and DNA replication in the normal human brain and Alzheimer's disease. *J. Neurosci.* **27**, 6859-6867.
Nakayama, K. I. and Nakayama, K. (2006). Ubiquitin ligases: cell-cycle control and cancer. *Nat. Rev. Cancer* **6**, 369-381.
Nakayama, K., Nagahama, H., Minamishima, Y. A., Matsumoto, M., Nakamichi, I., Kitagawa, K., Shirane, M., Tsunematsu, R., Tsukiyama, T., Ishida, N. et al. (2000). Targeted disruption of Skp2 results in accumulation of cyclin E and p27(Kip1), polyploidy and centrosome overduplication. *EMBO J.* **19**, 2069-2081.
Narbonne-Reveau, K., Senger, S., Pal, M., Herr, A., Richardson, H. E., Asano, M., Deak, P. and Lilly, M. A. (2008). APC/CFzr/Cdh1 promotes cell cycle progression during the Drosophila endocycle. *Development* **135**, 1451-1461.
Nishioka, N., Yamamoto, S., Kiyonari, H., Sato, H., Sawada, A., Ota, M., Nakao, K. and Sasaki, H. (2008). Tead4 is required for specification of trophectoderm in pre-implantation mouse embryos. *Mech. Dev.* **125**, 270-283.
Noda, S., Horiguchi, K., Ichikawa, H. and Miyoshi, H. (2008). Repopulating activity of ex vivo-expanded murine hematopoietic stem cells resides in the CD48-c-Kit+Sca-1+lineage marker- cell population. *Stem Cells* **26**, 646-655.
Papadantonakis, N., Makitalo, M., McCrann, D. J., Liu, K., Nguyen, H. G., Martin, G., Patel-Hett, S., Italiano, J. E. and Ravid, K. (2008). Direct visualization of the endomitotic cell cycle in living megakaryocytes: differential patterns in low and high ploidy cells. *Cell Cycle* **7**, 2352-2356.
Passegué, E., Wagers, A. J., Giuriato, S., Anderson, W. C. and Weissman, I. L. (2005). Global analysis of proliferation and cell cycle gene expression in the regulation of hematopoietic stem and progenitor cell fates. *J. Exp. Med.* **202**, 1599-1611.
Patel, S. R., Hartwig, J. H. and Italiano, J. E., Jr (2005). The biogenesis of platelets from megakaryocyte proplatelets. *J. Clin. Invest.* **115**, 3348-3354.
Reimann, J. D., Gardner, B. E., Margottin-Goguet, F. and Jackson, P. K. (2001). Emi1 regulates the anaphase-promoting complex by a different mechanism than Mad2 proteins. *Genes Dev.* **15**, 3278-3285.
Rossant, J. and Cross, J. C. (2001). Placental development: lessons from mouse mutants. *Nat. Rev. Genet.* **2**, 538-548.
Sakaue-Sawano, A., Kurokawa, H., Morimura, T., Hanyu, A., Hama, H., Osawa, H., Kashiwagi, S., Fukami, K., Miyata, T., Miyoshi, H. et al. (2008). Visualizing spatiotemporal dynamics of multicellular cell-cycle progression. *Cell* **132**, 487-498.
Sakaue-Sawano, A., Kobayashi, T., Ohtawa, K. and Miyawaki, A. (2011). Drug-induced cell cycle modulation leading to cell-cycle arrest, nuclear mis-segregation, or endoreplication. *BMC Cell Biol.* **12**, 2.
Schaeffer, V., Althauser, C., Shcherbata, H. R., Deng, W. M. and Ruohola-Baker, H. (2004). Notch-dependent Fizzy-related/Hec1/Cdh1 expression is required for the mitotic-to-endocycle transition in Drosophila follicle cells. *Curr. Biol.* **14**, 630-636.
Stuckey, D. W., Clements, M., Di-Gregorio, A., Senner, C. E., Le Tissier, P., Srinivas, S. and Rodriguez, T. A. (2011). Coordination of cell proliferation and anterior-posterior axis establishment in the mouse embryo. *Development* **138**, 1521-1530.
Ullah, Z., Kohn, M. J., Yagi, R., Vassilev, L. T. and DePamphilis, M. L. (2008). Differentiation of trophoblast stem cells into giant cells is triggered by p57/Kip2 inhibition of CDK1 activity. *Genes Dev.* **22**, 3024-3036.
Ullah, Z., Lee, C. Y., Lilly, M. A. and DePamphilis, M. L. (2009). Developmentally programmed endoreduplication in animals. *Cell Cycle* **8**, 1501-1509.
Vodermaier, H. C. (2004). APC/C and SCF: controlling each other and the cell cycle. *Curr. Biol.* **14**, R787-R796.
Zielke, N., Kim, K. J., Tran, V., Shibutani, S. T., Bravo, M. J., Nagarajan, S., van Straaten, M., Woods, B., von Dassow, G., Rottig, C. et al. (2011). Control of Drosophila endocycles by E2F and CRL4(CDT2). *Nature* **480**, 123-127.
Zybina, E. V. and Zybina, T. G. (1996). Polytene chromosomes in mammalian cells. *Int. Rev. Cytol.* **165**, 53-119.

Fig. S1. Validation experiments using EdU.
FACS analysis of DNA synthesis (EdU (Alexa 647)) and DNA content (DAPI) of TGCs (A and B) and MKCs (C and D) in comparison with postmitotic cells from forebrain (E and F). Cells with and without EdU incorporation (EdU(+) and EdU(-), respectively) (A, C, and E) were stained with DAPI for ploidy analysis (B, D, and F). Diploidy (2 C) is indicated by arrows (B, D, and F). The DNA contents of EdU(+) cells in the placenta (B) and bone marrow (D) occurred continuously, which suggests that our EdU procedure enabled labeling of only nuclei with intermediate DNA contents.

Fig. S2. Multi-color analysis of cell cycle regulation.
(A) The excitation (solid line) and emission (dotted line) spectra of DAPI (blue), mAG (green), mKO2 (red), and Alexa 647 (black). (B) Optical components used in the present study. 2P, two-photon excitation.

Fig. S3. A FulTrac well made of PDMS.
(A) A well containing Fucci-expressing cells was imaged using a 40× objective and 0.5× zoom lens. Fluorescence and DIC images were merged. The round culture area has a diameter of < 0.33 mm and is completely covered by the field of view of the 20× objective. (B) Schematic side view of a well. The stadium-shaped block permits all the light passing through the condenser (yellow) to reach the culture area. (C) Schematic top view of a PDMS block with four wells.

Fig. S4. Exposure to 10 μM etoposide induced NMuMG/Fucci2 cells to undergo endoreplication.
Fluorescence and DIC images were acquired using LCV100 microscopy and merged. Scale bar, 10 μm.

Fig. S5. TGCs labeled with Fucci fluorescence.
(Upper) Typical projection images of peripheral regions of placentas at E8.5, E9.5, E10.5, E11.5, E12.5, and E13.5 excised from Fucci transgenic mice (#504/#596). Tissues were fixed with 4% PFA and optically cleared with Sca*l*eU2 solution. Confocal images were taken by an AZ-C1 macro-zoom confocal microscope. (Lower) Automatic quantification (Volocity) of high ploidy cells in the periphery (nuclear volume > 150,000 μm^3) in a given cube 1.32 mm on each side. The 3D rendering software (Volocity) allowed us to distinguish the G1/S or endoG1/endoS yellow signals from overlapping signals in quantifying number of high ploidy cells.

Fig. S6. Preparation and characterization of hematopoietic cell fractions from #474/#610 mice.
(A) Hematopoietic cell lineage tree with cell surface markers for differentiation. (B) Flow cytometric profile of Fucci signals in HSC, MPP, mature B-cell, and immature B-cell fractions from the wild-type (WT) and #474/#610 double-transgenic mice. Single-cell suspensions were prepared and subjected to flow-cytometric analysis in order to analyze the levels of mAG and mKO2 signals. It is noted that the red level of mKO2 in the G0 state is several times higher than in the cycling G1 state. The differential intensity of red fluorescence between quiescent and proliferating cells was observed previously in the developing cerebral cortex of #596/#504 animals; postmitotic neurons in the cortical plate exhibited much brighter red fluorescence than mitotic neural progenitors in the ventricular zone, presumably due to accumulation of mKO2-hCdt1(30/120) after cell-cycle exit (Sakaue-Sawano et al. 2008*). Likewise, HSCs and mature B-cells from #474/#610 stayed mostly in quiescent G0 phase, while a substantial fraction of MPP cells or immature B-cells from the transgenic mice were cycling. (C) Typical fluorescence and DIC images of Fucci-expressing cells at DIV 4, 6, and 8 originating in MPP, CMP, and MKC fractions. Scale bar, 10 μm.

*Sakaue-Sawano A, Kurokawa H, Morimura T, Hanyu A, Hama H, Osawa H, Kashiwagi S, Fukami K, Miyata T, Miyoshi H, et al. 2008. Visualizing spatiotemporal dynamics of multicellular cell-cycle progression. *Cell* **132:** 487-498.

Fig. S7. A series of images of HSCs in a FulTrac well, which differentiated into MKCs in the presence of thrombopoietin (the same cell samples as in Movie S3).
Time-lapse imaging was performed by an LCV100 microscope for 269 hours. Scale bar, 100 μm.

Fig. S8. Snapshots of MKBs and MKCs that emerged from an HSC fraction.
These cells had single multilobular nuclei with green (endoS/G2) or red (endoG1) fluorescence. Scale bar, 10 μm.

Fig. S9. A series of images of an MKB in a FulTrac well, which differentiated into an MKC in the presence of thrombopoietin (tracked from Movie S4).
(A) (top), The endomitotic cycling of an MKB with increasing chromatin values from estimated 2 C to 16 C. Fucci fluorescence images and DIC images were merged. (bottom), Cell cycle time duration of alternating green and red nuclei of the observed MKB. (B) Nine images in (A) were magnified. The green fluorescence spread over the entire cell (image 2, 5 and 8), indicating a breakdown of the nuclear envelope. Scale bars, 10 μm.

Fig. S10. The endomitotic cycling of an MKB derived from an MEP fraction.
As its C value increased from 8 C to 16 C, the latency time for the emergence of red (endoG1) was prolonged. Fucci fluorescence images and DIC images were merged. Scale bar, 10 μm.

Placental cells from a #504/#596 mouse

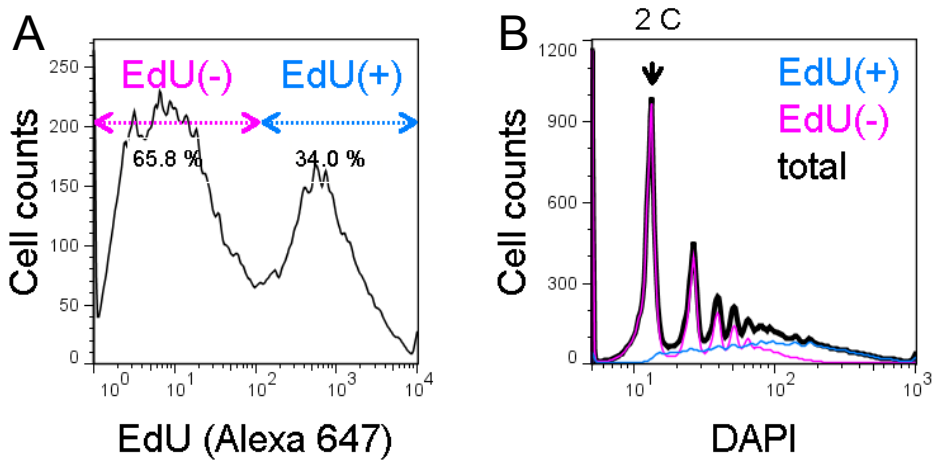

TPO-treated bone marrow cells from a #474/#610 mouse

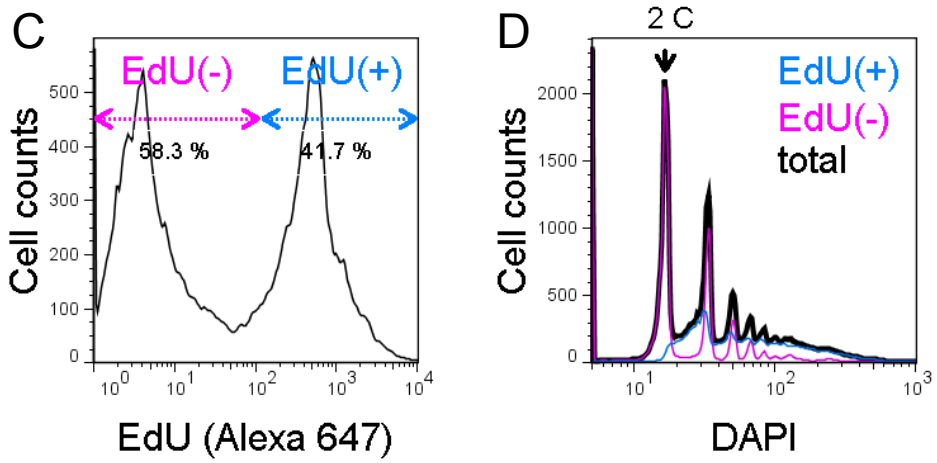

Cells from an adult mouse brain

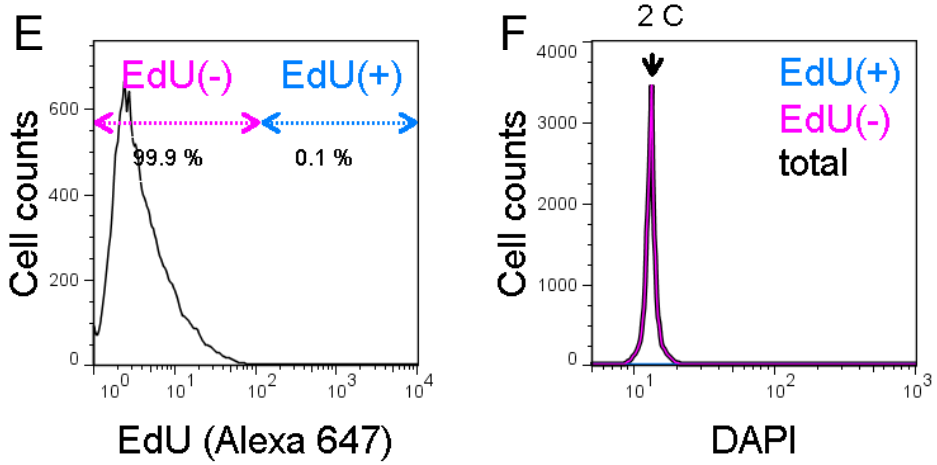

A

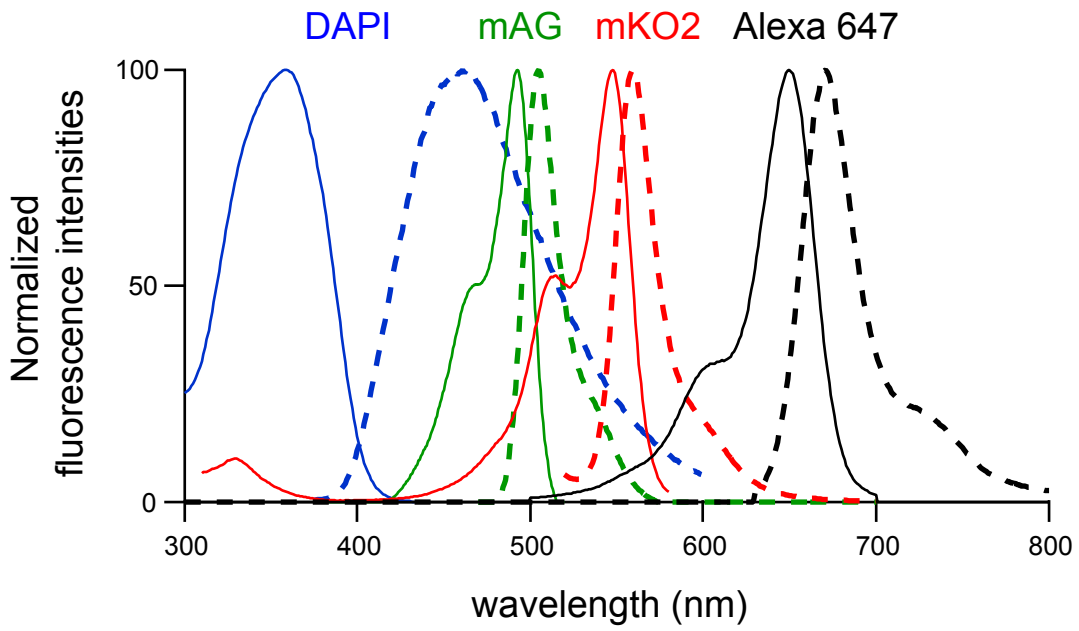

B

		DNA content	Fucci		EdU	
		DAPI	mAG	mKO2	Alexa 647	
BD FACSAriaII	excitation	355 nm	488 nm	561 nm	640 nm	Figs. 1, S1
	emission	450/50BP	530/30BP	610/20BP	710/50BP	
Olympus LCV100	excitation	-	470DF35	BP520-540HQ	-	Figs. 3, 5, S3, S4, S6C, S7, S9, S10
	emission	-	510WB40	BP555-600HQ	-	
Olympus FV1000	excitation	405 nm	473 nm	559 nm	-	Figs. 4B, S8
	emission	415 - 480	483 - 513	570 - 630	-	
Nikon AZ-C1	excitation	-	488 nm	561 nm	-	Figs. 4C-M, S5
	emission	-	525/50	595/40	-	
Zeiss LSM 780	excitation	780 nm (2P)	488 nm	561 nm	633 nm	Fig. 2
	emission	382 - 488	491 - 534	569 - 631	638 - 735	

Sakaue-Sawano_Fig S3.

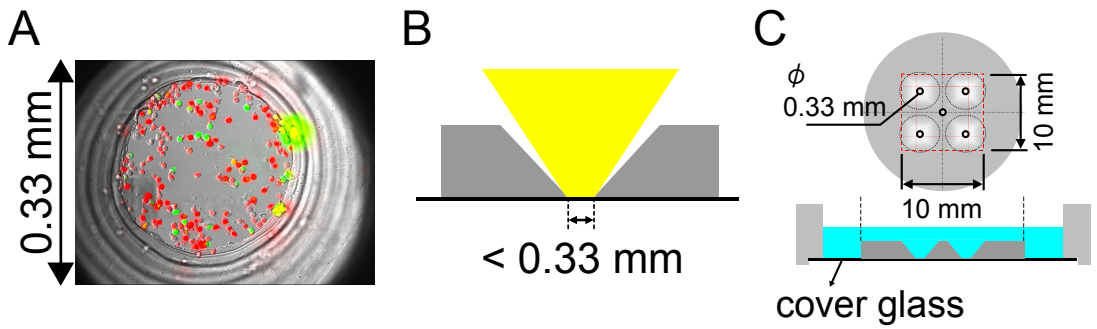

NMuMG/Fucci2, 10 μM etoposide 18 min interval

green, ~ 4 C (G2) → red, 4 C (endoG1)

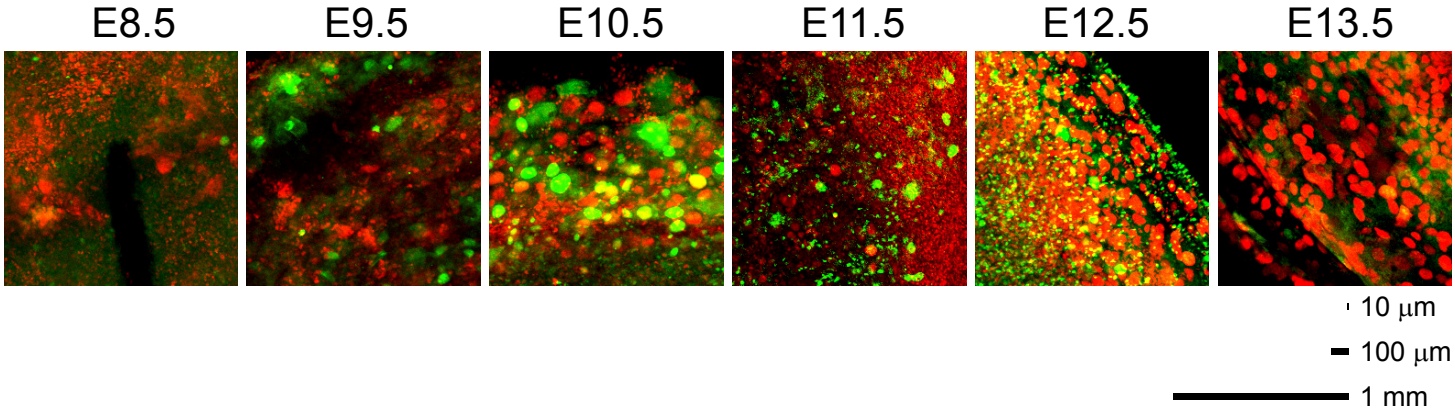

number of high ploidy cells (nuclear volume > 150,000 μm³)

	E8.5	E9.5	E10.5	E11.5	E12.5	E13.5
endoS/G2 (green)	0 (0)	7 (87.5)	25 (56.8)	19 (33.9)	5 (8.1)	1 (0.8)
endoG1/S (yellow)	0 (0)	0 (0)	3 (6.8)	3 (5.3)	1 (1.6)	0 (0)
endoG1 (red)	10 (100)	1 (12.5)	16 (36.3)	34 (60.7)	56 (90.3)	120 (99.2)
total	10	8	44	56	62	121

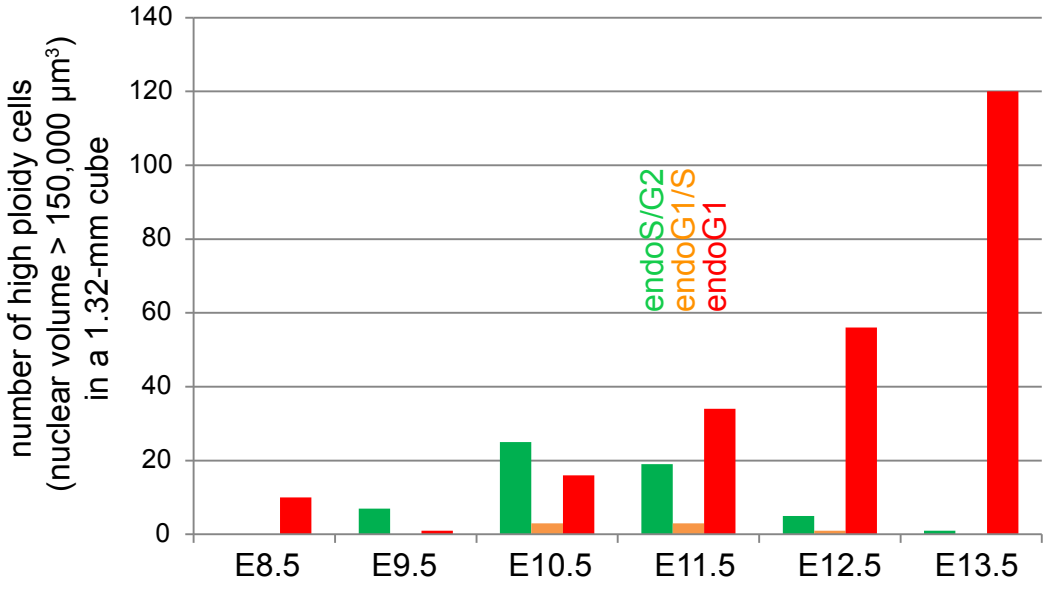

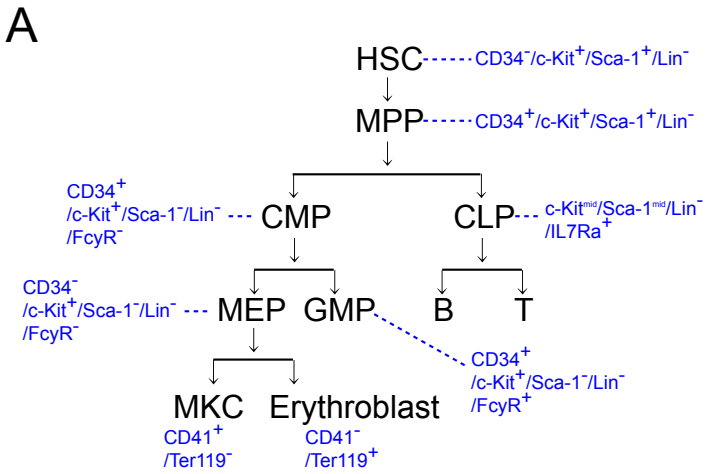
A
HSC
CD34-/c-Kit+/Sca-1+/Lin-
MPP
CD34+/c-Kit+/Sca-1+/Lin-
CD34+ /c-Kit+/Sca-1-/Lin- /FcyR-
CMP
CLP
c-Kitmid/Sca-1mid/Lin- /IL7Ra+
CD34- /c-Kit+/Sca-1-/Lin- /FcyR-
MEP
GMP
B
T
CD34+ /c-Kit+/Sca-1-/Lin- /FcyR+
MKC
Erythroblast
CD41+ /Ter119-
CD41- /Ter119+

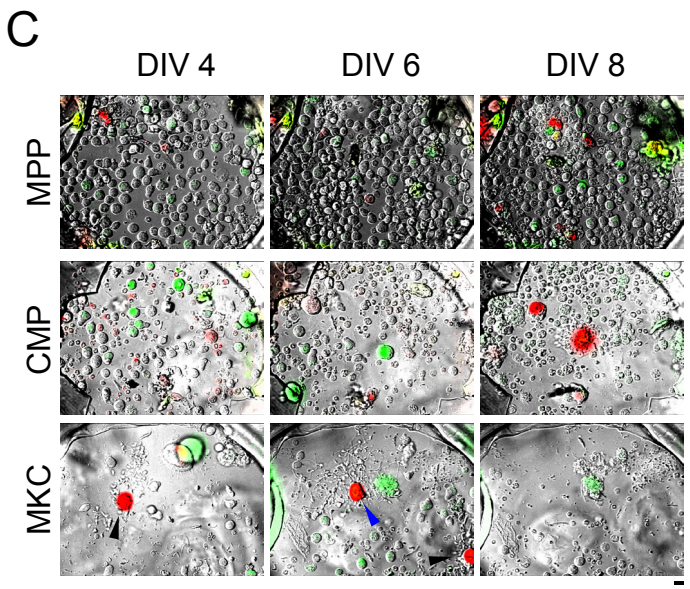
C
DIV 4
DIV 6
DIV 8
MPP
CMP
MKC

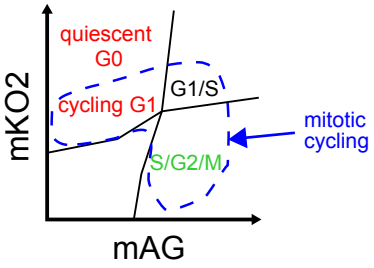
B
quiescent G0
cycling G1
G1/S
S/G2/M
mitotic cycling
mKO2
mAG

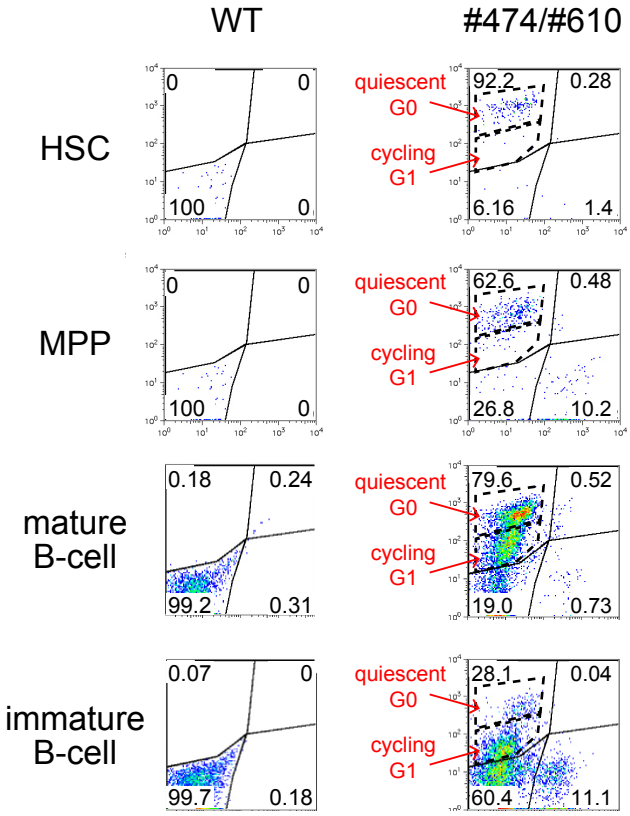
WT
#474/#610
HSC
MPP
mature B-cell
immature B-cell
quiescent G0
cycling G1
0
100
92.2
0.28
6.16
1.4
62.6
0.48
26.8
10.2
0.18
0.24
99.2
0.31
79.6
0.52
19.0
0.73
0.07
99.7
0.18
28.1
0.04
60.4
11.1

HSC fraction, DIV 1 ~

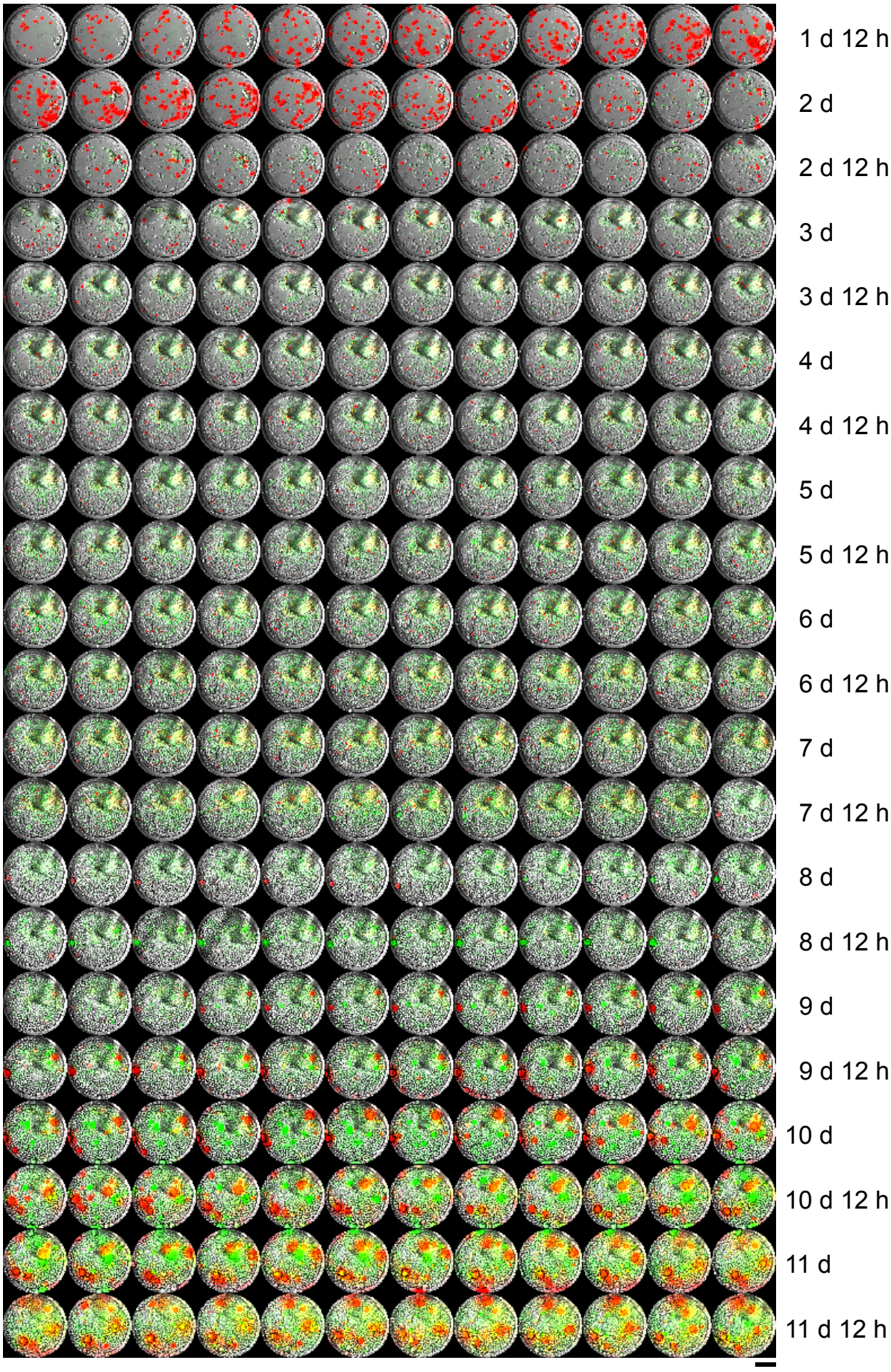

Sakaue-Sawano_Fig S8.

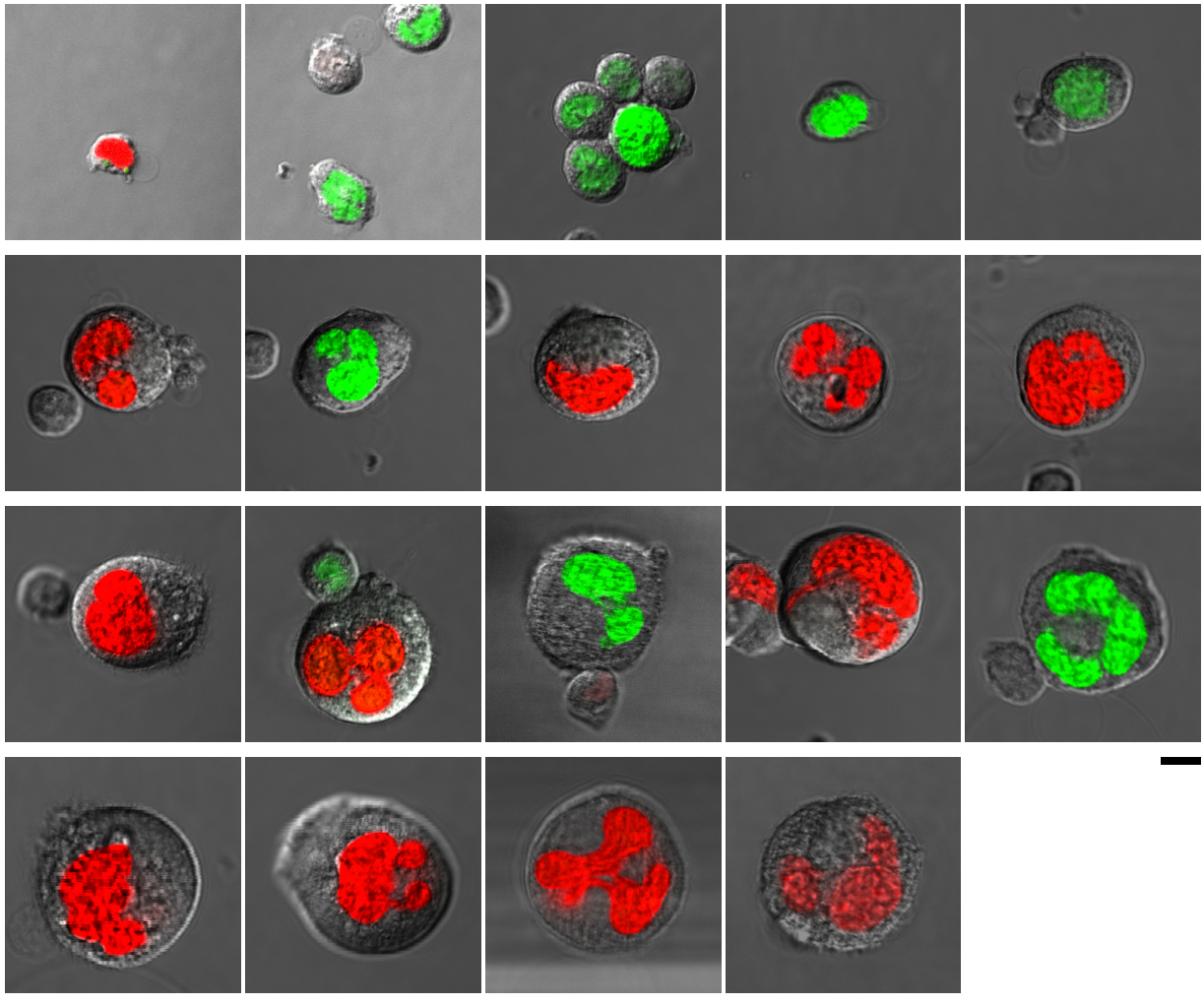

A

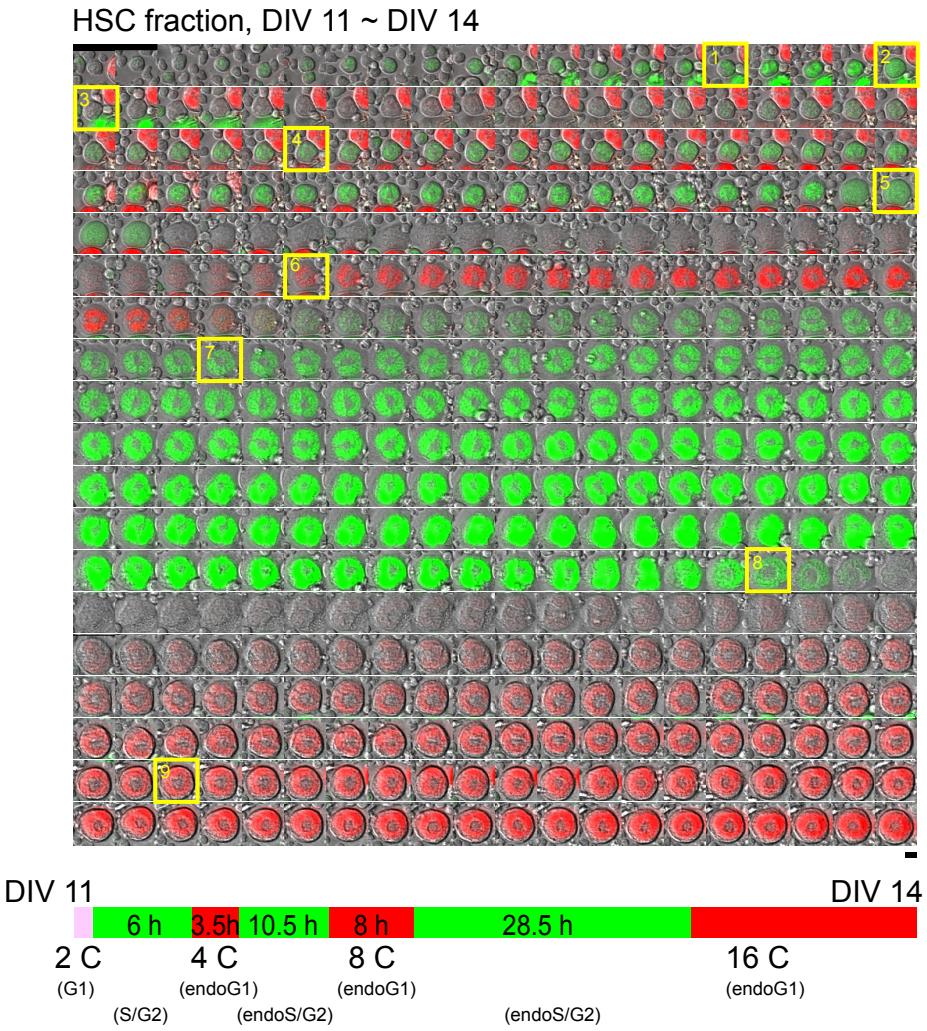
HSC fraction, DIV 11 ~ DIV 14
1
2
3
4
5
6
7
8
9
DIV 11
DIV 14
6 h
3.5h
10.5 h
8 h
28.5 h
2 C
(G1)
4 C
(S/G2)
(endoG1)
(endoS/G2)
8 C
(endoG1)
(endoS/G2)
16 C
(endoG1)

B

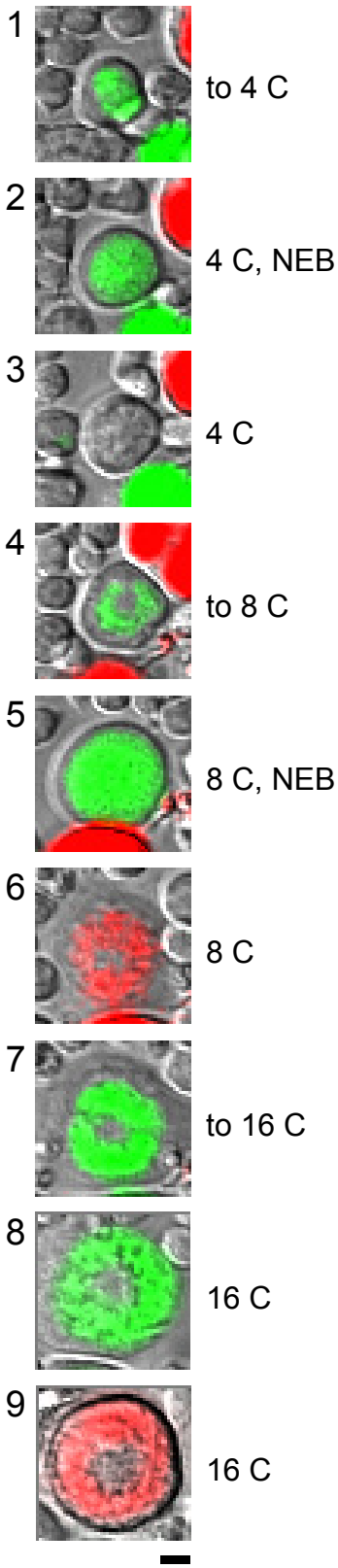
1
to 4 C
2
4 C, NEB
3
4 C
4
to 8 C
5
8 C, NEB
6
8 C
7
to 16 C
8
16 C
9
16 C

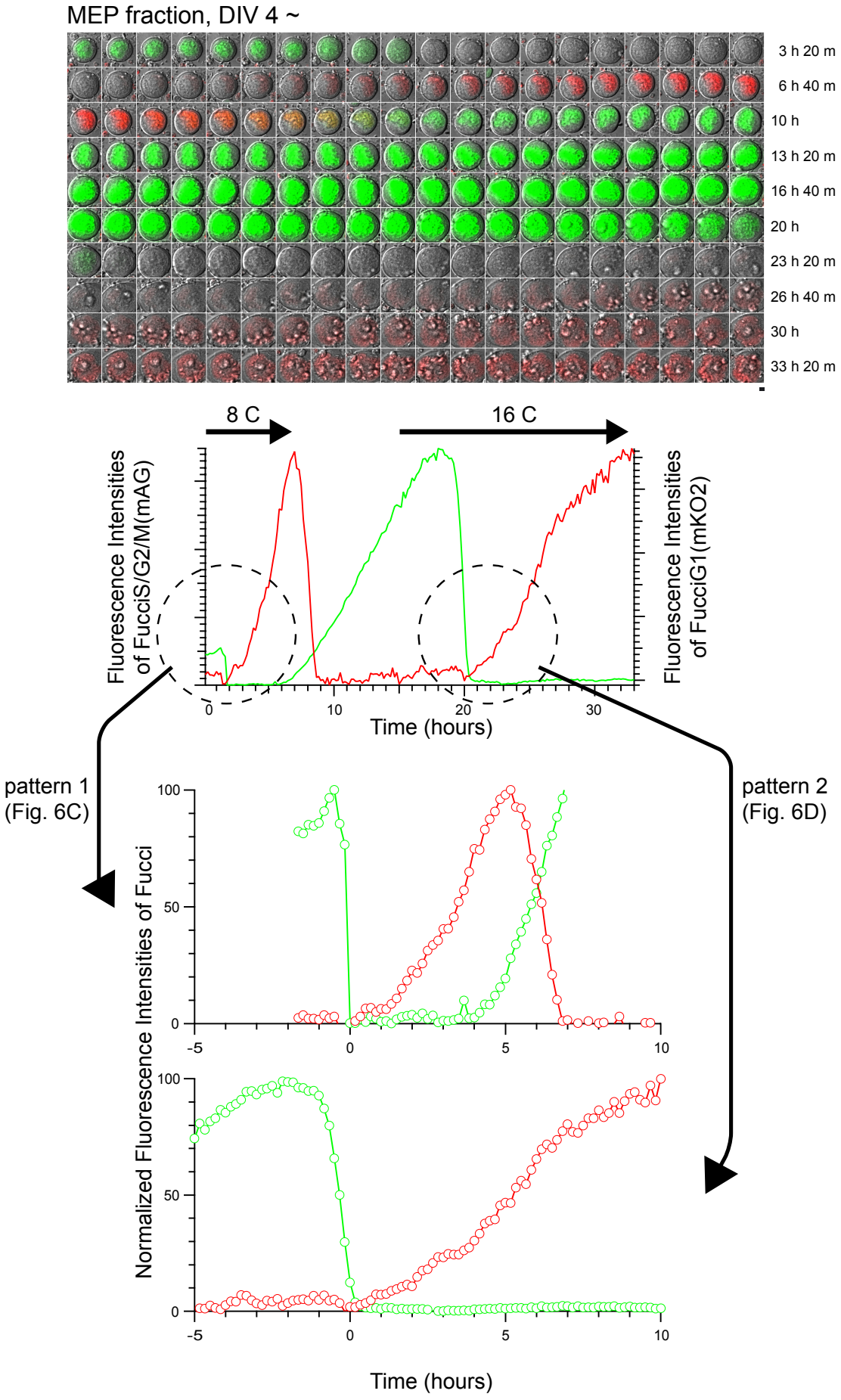
MEP fraction, DIV 4 ~
3 h 20 m
6 h 40 m
10 h
13 h 20 m
16 h 40 m
20 h
23 h 20 m
26 h 40 m
30 h
33 h 20 m
8 C
16 C
Fluorescence Intensities of FucciS/G2/M(mAG)
Fluorescence Intensities of FucciG1(mKO2)
0
10
20
30
Time (hours)
pattern 1 (Fig. 6C)
pattern 2 (Fig. 6D)
Normalized Fluorescence Intensities of Fucci
100
50
0
-5
0
5
10
Time (hours)

Movie S1. Time-lapse imaging of early embryogenesis (Related to Fig. S3).
A wild-type mouse embryo (morula stage) was grown on a FulTrac well, and time-lapse imaging was performed using an LCV100 microscope. Images were acquired every 25.6 minutes. Total imaging time = 81 hours.

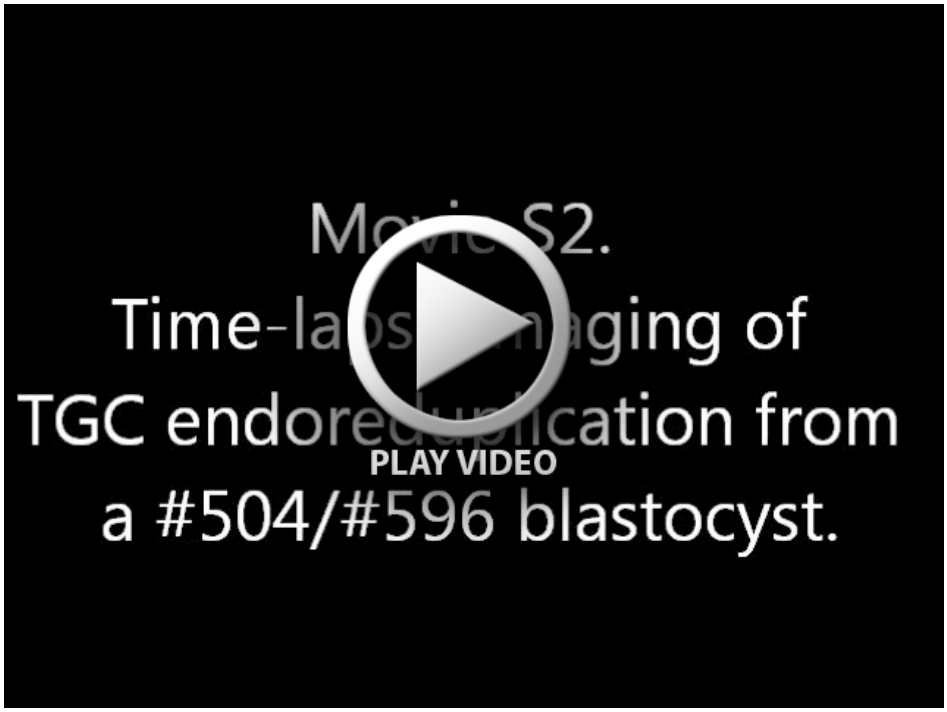

Movie S2. Time-lapse imaging of TGC endoreduplication from a #504/#596 blastocyst (Related to Fig. 3).
A Fucci transgenic mouse (#504/#596) blastocyst was grown on a FulTrac well, and time-lapse imaging was performed using an LCV100 microscope. Images were acquired every 20 minutes. Timestamp "0" means the time point when the medium was changed to RPMI1640/20%FBS. Total imaging time = 188 hours.

Movie S3. Time-lapse imaging of MKC endomitosis (Related to Fig. 5 and Fig. S7).
HSCs from a Fucci transgenic mouse (#474/#610) were grown on a FulTrac well, and time-lapse imaging was performed using an LCV100 microscope. Images were acquired every 4 minutes. The time stamp shows the time when the cell sorting was performed. Total imaging time = 269 hours.

Movie S4. Time-lapse imaging of MKC endomitosis (Related to Fig. 5 and Fig. S9).
HSCs from a Fucci transgenic mouse (#474/#610) were grown on a FulTrac well and time-lapse imaging was performed using an LCV100 microscope. Images were acquired every 66 minutes. The time stamp shows the time when the cell sorting was performed. Total imaging time = 219 hours.